2012

Investigating the structural evolution of thiolate protected gold clusters from first-principles

Yong Pei
Xiangtan University, ypnku78@gmail.com

Xiao Cheng Zeng
University of Nebraska-Lincoln, xzeng1@unl.edu

Nanoscale

Cite this: *Nanoscale*, 2012, **4**, 4054

www.rsc.org/nanoscale

REVIEW

Investigating the structural evolution of thiolate protected gold clusters from first-principles

Yong Pei*[a] and Xiao Cheng Zeng*[b]

Received 21st March 2012, Accepted 18th April 2012
DOI: 10.1039/c2nr30685a

Unlike bulk materials, the physicochemical properties of nano-sized metal clusters can be strongly dependent on their atomic structure and size. Over the past two decades, major progress has been made in both the synthesis and characterization of a special class of ligated metal nanoclusters, namely, the thiolate-protected gold clusters with size less than 2 nm. Nevertheless, the determination of the precise atomic structure of thiolate-protected gold clusters is still a grand challenge to both experimentalists and theorists. The lack of atomic structures for many thiolate-protected gold clusters has hampered our in-depth understanding of their physicochemical properties and size-dependent structural evolution. Recent breakthroughs in the determination of the atomic structure of two clusters, $[Au_{25}(SCH_2CH_2Ph)_{18}]^q$ ($q = -1, 0$) and $Au_{102}(p\text{-MBA})_{44}$, from X-ray crystallography have uncovered many new characteristics regarding the gold–sulfur bonding as well as the atomic packing structure in gold thiolate nanoclusters. Knowledge obtained from the atomic structures of both thiolate-protected gold clusters allows researchers to examine a more general "inherent structure rule" underlying this special class of ligated gold nanoclusters. That is, a highly stable thiolate-protected gold cluster can be viewed as a combination of a highly symmetric Au core and several protecting gold–thiolate "staple motifs", as illustrated by a general structural formula $[Au]_{a+a'}[Au(SR)_2]_b[Au_2(SR)_3]_c[Au_3(SR)_4]_d[Au_4(SR)_5]_e$ where a, a', b, c, d and e are integers that satisfy certain constraints. In this review article, we highlight recent progress in the theoretical exploration and prediction of the atomic structures of various thiolate-protected gold clusters based on the

[a]*Department of Chemistry, Key Laboratory of Environmentally Friendly Chemistry and Applications of Ministry of Education, Xiangtan University, Hunan Province, China 411105. E-mail: ypnku78@gmail.com*

[b]*Department of Chemistry and Nebraska Center for Materials and Nanoscience, University of Nebraska-Lincoln, Lincoln, Nebraska, 68588, USA. E-mail: xzeng1@unl.edu*

Yong Pei

Yong Pei received his BSc degree from the Deptartment of Chemistry, Xiangtan University, China (Hunan) in 2001. He obtained a PhD degree from Nanjing University, China (Nanjing) in 2006. After postdoctoral research at the University of Nebraska_Lincoln, he joined the Chemistry faculty of Xiangtan University in 2010. His current research interests include the methodological development of global search algorithms for complicated ligand protected metal clusters and theoretical studies on the structure, optical, catalytic, and magnetic properties of metal nanoparticles.

Xiao Cheng Zeng

Xiao Cheng Zeng is Ameritas Distinguished University Professor at the University of Nebraska-Lincoln, USA, a fellow of the American Association for the Advancement of Science, a fellow of the American Physical Society, a former John Simon Guggenheim fellow and a recipient of the American Chemical Society Midwest Award. He has published 296 papers in refereed journals (h-index: 41), and supervised 20 graduate students (14 PhD and 6 MS) and 20 postdoctoral fellows. Zeng received his BS from Peking University, PhD from Ohio State University and performed postdoctoral research at University of Chicago and UCLA.

"divide-and-protect" concept in general and the "inherent structure rule" in particular. As two demonstration examples, we show that the theoretically predicted lowest-energy structures of $Au_{25}(SR)_8^-$ and $Au_{38}(SR)_{24}$ (–R is the alkylthiolate group) have been fully confirmed by later experiments, lending credence to the "inherent structure rule".

1 Introduction

The strong relativistic effect of Au results in more significant s–d hybridization than other coinage metals, which leads to many novel structures and properties for nanosized gold clusters. For gas-phase gold clusters (Au_N^q, $q = 0, \pm1$, $N \leq 60$), significant advances have been made through combined experimental and theoretical efforts over the past two decades, which provide deeper insights into their size-dependent atomic structures, and thereby the critical information needed for understanding the structure–size–property relationship.[1–10] The combination of global optimization algorithms and density functional theory[11,12] (DFT) calculation has been proven to be a powerful tool to generate structures of low-energy gold clusters, as well as for the determination of the lowest-energy structure by comparing computed photoelectron spectra with the experimental spectra. For example, unique structural transitions for gold cluster anions in the size range of $N = 14$–20 have been revealed, *e.g.*, from the flat cage to hollow cage and to tetrahedral pyramid.[1–3] However, the determination of the atomic structure for ligand-protected gold clusters is still a grand challenge to both experimentalists and theoreticians, largely due to the complexity of the ligand shell.

The thiolate-protected gold nanoparticles (RS-AuNPs) or nanoclusters entail a distinctive quantum confinement effect, as well as many size-dependent physicochemical properties and functionalizations, such as magnetism, catalysis, enhanced photoluminescence, sizeable optical absorption or HOMO–LUMO gap, electrochemical properties, and high stability at magic numbers.[13–17] The first experimental method for synthesizing RS-AuNPs was demonstrated by Brust *et al.* in 1994.[18] Although many variants of the original method were subsequently developed,[19] the key route is essentially the same, i.e., to involve the reduction of high valence Au salts. However, the RS-AuNPs synthesized from these methods are usually a mixture of different sizes, which require further separation for structural and compositional analysis. During the past fifteen years or so, most experimental efforts were devoted to resolving the chemical composition of RS-AuNPs.[20–54] In particular, gold nanoparticles in the size range of subnanometre to ~2 nm have attracted most interest. Due to the difficulty in crystallization of RS-AuNPs, few structures of RS-AuNPs have been fully resolved, which has greatly hindered an in-depth understanding of the structure–property relationship of RS-AuNPs.

The gold–phosphane–halide clusters are one of few examples of ligand-protected gold clusters whose structures have been well resolved in experiments.[55–58] The Au cores in these gold–phosphane–halide clusters exhibit ordered and uniform packing pattern so that a typical structural pattern for these clusters can be described as a symmetric Au core plus protecting ligands. Mingos *et al.* pointed out that the coordination of ligands to gold clusters may promote a more favorable hybridization among metal–atom orbitals and result in stronger radial metal–metal bonding, leading to a major structural transition of the gold clusters.[59] Theoretical efforts for the exploration of structures of RS-AuNPs date from 1999. Before 2008, due to the lack of a precise atomic structure of any RS-AuNPs, earlier theoretical models of RS-AuNPs, *e.g.* $Au_{38}(SR)_{24}$, mainly followed the "conventional" structural pattern attained based on gold–phosphane–halide clusters, which is typically a combination of a ligand and an intact symmetric Au core.[60] More specifically, the Au atoms were assumed to arrange into a compact core and the –RS ligand sticks to the Au core on the atop, bridge, or triangle site. Such a conventional model of Au–SR linkage has prevailed for a long time in the study of the interfacial structure of self-assembled thiol monolayers on gold surfaces.[61] Although some theoretical studies have suggested that the ligand/Au core interfacial structure in RS-AuNPs could be quite different from the conventional model of metal–ligand linkage, no general structural rule was proposed due largely to the lack of experimentally determined structures.[62,63]

The successful crystallization of $Au_{102}(p\text{-MBA})_{44}$ has been a huge motivation for recent RS-AuNP research, especially due to the finding of unexpected atomic structure.[64] For the first time, a clear picture of the gold–sulfur bonding in an RS-AuNP was revealed, *i.e.*, the –SR group is not merely adsorbed on the surface of an Au core to form a single Au–S linkage; rather, it can strongly disturb the surface structure of the Au core and lead to the formation of novel gold-thiolate protecting units (coined as "staple motif") on a highly symmetric Au core. It is worthy of quoting one sentence in a perspective article by Whetten *et al.* on the structure of $Au_{102}(p\text{-MBA})_{44}$:[65] "The known properties of nanoscale clusters can now be rationalized in terms of atomic ordering." The term "atomic ordering" was also applicable in describing another successfully crystallized thiolate-protected gold cluster, $Au_{25}(SCH_2CH_2Ph)_{18}^-$.[66,67] On the basis of the known atomic structures of $Au_{102}(p\text{-MBA})_{44}$ and $Au_{25}(SCH_2CH_2Ph)_{18}^-$, a plausible "inherent structural rule" about the formation of RS-AuNPs has been introduced, namely, any RS-AuNP can be viewed as a combination of a highly symmetric Au_N-core with several protection staple motifs, as represented by a general structural formula $[Au]_{a+a'}[Au(SR)_2]_b[Au_2(SR)_3]_c[Au_3(SR)_4]_d[Au_4(SR)_5]_e$ where a, a', b, c, d and e are integers that satisfy certain constraints.[63] This view is also consistent with the "divide-and-protect" concept.[63] Over the past few years, this structural rule has been successfully applied to the structural prediction of several thiolate-protected gold clusters. In this review article, our focus will be placed on recent theoretical progress in the structural prediction of thiolate (–RS) protected gold clusters on the basis of the "inherent structure rule", combined with other structural search methods and density functional theory (DFT) calculations.

This article is organized as follows: Section 2 discusses the major difficulties encountered for the structural prediction of thiolate-protected gold clusters. Section 3 summarizes earlier studies of the $Au_{38}(SR)_{24}$ cluster, followed by a summary of the

recent breakthrough in the structure determination of $Au_{102}(p\text{-}MBA)_{44}$ and $Au_{25}(SCH_2CH_2Ph)_{18}^{-}$, and by an illustration of the "inherent structure rule" that will be utilized for the structural prediction of various thiolate-protected gold clusters. Section 4 elucidates some details about the intrinsic connection between the cluster's geometric structure and electronic properties, including the origin of electronic magic numbers. Finally, we briefly review the structure–activity relationship for the thiolate-protected gold clusters with an example of catalytic oxygen activation. Note that in this article we mainly focus on the structural aspects of thiolate-protected gold clusters: other properties derived from the electronic effects such as optical absorption are not fully discussed. The readers can refer to recently published review articles by Aikens, Jiang, and Häkkinen for more information about the electronic structures and optical absorption spectra of thiolate-protected gold clusters.[68–70]

2. Challenges in structural prediction for RS-AuNPs

2.1 Potential energy surface and global optimization algorithms

The potential energy surface (PES) can be described by a mathematical potential function whose values are the potential energies of a system. For the PES of a molecule or a cluster, the atomic positions are represented as the variables of the potential function, while the values of the function are the corresponding potential energies. Two forms of potential functions of gold have been widely used in the study of gold clusters: (1) a parameterized classical many-body potential (such as Sutton–Chen[71] and Gupta[72] potential functions) and (2) the total energy calculated using *ab initio* and density-functional theory methods. For the former, the potential function is represented by an analytical mathematical function including a few pre-defined parameters. A major advantage of such a parameterized potential function (or force field) is its high computation efficiency, and this form of potential function has been commonly used in the study of the structures of gold clusters since the 1990s.[73,74] A disadvantage of the classical potential function is that the pre-defined parameters are inadequate to fully address electronic effects in gold clusters. The quantum mechanical methods such as density functional theory methods[11,12] yield more genuine PES and have been generally used in studying structures and properties of small-sized gold clusters since the 1970s. The foremost information that can be obtained from solving the Schödinger equation is the electronic energy for given atomic positions of molecules and clusters. To reduce computational costs, the Born–Oppenheimer (BO) approximation is usually applied, which assumes the positions of nuclei are fixed while computing electronic properties.[75] The resulting hyper-PES as a function of the atomic positions is the so-called BO-PES.

The lowest point on a PES is referred to as the global minimum. For a cluster, the global minimum corresponds to the most stable structure of the cluster, which is generally believed to be the observed structure in experiments. The search for the global minimum on the PES is therefore equivalent to the determination of the most stable structure of a cluster. However, locating the global minimum on a complicated hyper-PES is a grand challenge due to the existence of a huge number of local minima for medium- to large-sized clusters. The genetic-algorithm (GA),[76] simulating annealing (SA),[77] and basin-hopping (BH)[78] are three popular methods for seeking the global minimum of an atomic cluster. The GA method explores the cluster structure by modeling some aspects of biological evolution. For example, a population of clusters evolves toward low energy through mutation and mating of structures, along with the selection of those with low potential energy. As a result, new configurations are produced *via* "genetic manipulation" combined with a local optimization algorithm such as the conjugate gradient method. SA method takes advantage of the relatively less complex free-energy landscape at high temperatures and attempts to follow the free energy global minimum as the temperature is decreased. A difficulty with the SA approach is that, if the free-energy global minimum changes at low temperatures where dynamical relaxation is slow, the algorithms will become confused by the structure corresponding to the high temperature free energy global minimum. The BH method, originally proposed by Wales and Doye, has been widely used in predicting the global-minimum structure of bare gold clusters Au_N^- with N up to 58.[2–10] In the BH method, the transformation maps the potential function onto a series of plateaus where the barriers between local minima can be removed, as shown in Scheme 1. A series of Monte Carlo random walks are normally used to explore the PES, combined with a local optimization method to locate local minima. Once a local minimum is located, the next step is to perform a hopping (or a random walk) to explore new configurations on the PES.

However, direct application of the three global optimization methods has encountered computational difficulties in the case of thiolate-protected gold clusters due largely to the presence of organic ligands, which dramatically increases the computational cost and time required to locate the global minimum. In addition, many global optimization methods typically require random moves of atomic positions rather than a fraction of ligand. In reality, the organic ligands tend to stay outside the metal core, which also requires modification of the algorithm to take such physical effects into account. Hence, the "inherent structure rule" for the thiolate-protected gold clusters summarized from recent experiments[65–67] can be viewed as an insight-based, highly efficient, and low-cost search method to seek the true global minima

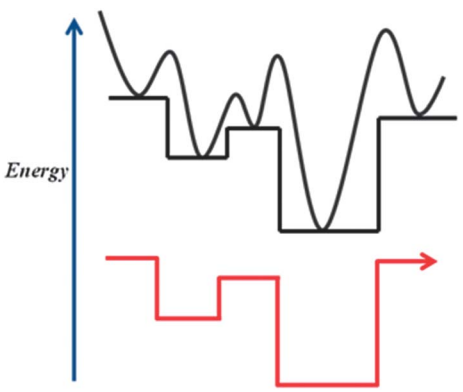

Scheme 1 A schematic diagram illustrating the energy transformation for a one-dimensional potential energy surface. The black curve is the original potential energy surface and the red line is the transformed energy basin map.

of thiolate-protected gold clusters without the expensive enumeration of cluster structures.

2.2 Information required for predicting the structure of a complex RS-AuNP

To predict the lowest-energy structure of small-sized gas-phase gold clusters from theory, low-lying isomers (typically several hundred) are attained using a combined global optimization method and DFT calculations.[2–10] Moreover, comparison with experimental data such as a photoelectron spectrum of anionic clusters is a key step to determine the structures of the most stable clusters. For medium-sized thiolate-protected gold clusters, the generation of low-lying structures from DFT calculations is computationally very expensive. Furthermore, relative energies predicted from DFT calculations are also affected by the exchange-correlation functional and basis set. Therefore, additional evidence is needed to support the predicted low-energy clusters. For example, the UV-vis absorption spectra have been often used to provide information on the optical absorption edge, feature absorption peaks, and the shape of optical curves, which are very sensitive to the structure and composition of the cluster. The optical absorption curves can therefore provide one set of experimental evidences for validating theoretical predictions. In principle, UV-vis absorption spectra originate from the excitation of electrons from the ground state, including the singlet-to-singlet transition and singlet-to-triplet transitions. Theoretically, the excitation energy of a thiolate gold cluster can be computed using time-dependent DFT (TDDFT) methods.[79] For nanosized gold clusters, it has been found that the excitation of electrons involves mainly singlet-to-singlet transitions. Therefore, good agreement between the theoretical excitation energy curve and the experimental optical absorption spectrum is necessary to validate the theoretically predicted thiolated gold cluster.

In addition, the experimental powder X-ray diffraction (XRD) curve is an auxiliary data to further validate the theoretically predicted cluster structure. The theoretical XRD curve can be obtained using the Debye formula with the atomic distance (for the cluster studied) as the input:

$$I(s) = \sum_i \sum_{j \neq i} \frac{\cos\theta}{(1 + \alpha\cos 2\theta)} \exp\left(-\frac{Bs^2}{2}\right) f_i f_j \frac{\sin(2\pi d_{ij})}{2\pi d_{ij}}$$

where s is the diffraction vector length and θ is the scattering angle, satisfying $s = 2\sin\theta/\lambda$. The λ and α are determined by the experimental set-up. B is the damping factor, which reflects thermal vibrations. The corresponding atomic numbers are used for the scattering factors f_i. d_{ij} is the distance between atoms i and j. However, the XRD curve is not as sensitive to the cluster structure as the optical absorption spectrum, especially if the structural difference between the Au-cores of two isomers is small.

3. Structural prediction of thiolate-protected gold clusters from the "inherent structure rule"

3.1 Earlier structural models of $Au_{38}(SR)_{24}$ and the "divide-and-protect" concept

The $Au_{38}(SR)_{24}$ cluster deserves special mention because many theoretical predictions were published long before the experimental confirmation, which reflects the progress in the research of the structure of RS-AuNPs. In 1996, Luedtke and Landman reported the first theoretical study of the structural, dynamic, and thermodynamic properties of passivated gold nanocrystallites $Au_N(SR)_M$, with N = 140, 201, 459, and 586, using classical molecular mechanics (MM) and force field based molecular dynamics (MD) modeling.[80] They showed that the coordination of thiol molecules on the surface of finite-sized gold crystallites may differ from that on bulk surfaces, depending on the size and geometry of the crystallites. It was also suggested that the gold nanocrystallites maintain an intact structure with the presence of thiol ligands. Wilson and Johnston introduced an alternative Au cluster/thiol–ligand interaction model based on the MM method to describe the surface passivation effects on gold clusters.[81] It was suggested that surface passivation by thiol ligands results in changes in the order of stability of Au clusters compared to Au clusters observed in the gas-phase. In particular, the icosahedron-based core structure was predicted to be more stable than fcc-like cuboctahedral or truncated octahedral geometries for thiol-protected Au_{38} and Au_{55} clusters.

The $Au_{38}(SR)_{24}$ cluster also appears to be the first thiolate-protected gold cluster studied *via ab initio* calculations. The composition of $Au_{38}(SR)_{24}$ was first reported by Whetten and co-workers in 1997 from their mass spectrometric experiments.[14,20] However, the internal atomic structure has puzzled both experimentalists and theorists for more than ten years. Since 1999, more theoretical efforts have been made to explain the unique stability and structure of $Au_{38}(SR)_{24}$ from *ab initio* calculations. In the first structural model proposed by Häkkinen *et al.*, a truncated octahedron Au_{38} containing 6 square Au_4 units on the Au core surface was constructed with 24 –RS groups evenly distributed on the surface of the Au core. The structural relaxation based on a plane-wave density-functional theory and pseudopotential method (Born–Oppenheimer local-spin-density molecular dynamics) led to a local-minimum structure with the high-symmetry Au_{38} core unchanged.[60] Additional electronic structure analysis of the optimized cluster revealed notable electron transfer from gold to sulfur. The Au core was positively charged. Majumder and Larsson and their co-workers employed a similar ligand adsorption pattern to study the interactions between thiol groups and nano-sized gold clusters *via ab initio* calculations. They found the structure of the Au core was only slightly affected by the thiolate ligands.[82,83]

Garzón *et al.* demonstrated that the thiol monolayer may have a much stronger structural effect on the Au core through observing the structural relaxation of an $Au_{38}(SR)_{24}$ model based on the DFT calculations.[62] Interestingly, the S-head of the thiolate ligands was found to significantly penetrate into the Au core, strongly affecting not only the symmetry of the Au core but also the core/ligand interfacial structure. A mixture of ligand motifs on the cluster surface, including –RS–Au–SR– and –RS–Au–SR–Au–SR– motifs, were proposed for the first time. In fact, a novel gold-substrate sulfur-headgroup interfacial structure for the self-assembled monolayers on Au(111), named as "staple motif" was also recognized at the time,[84] which co-indicated the strong bonding interactions between gold and sulfur at the interface. These results called for new physical pictures to understand the interfacial structure of RS-AuNPs.

Inspired by earlier theoretical predictions of $Au_{38}(SR)_{24}$ structure and concurrent experimental findings of novel –RS–Au–RS– motifs on the Au surface, Häkkinen *et al.* introduced in 2006 a new concept to understand the structure of thiol group-protected gold nanoparticles, namely, the "divide-and-protect" concept.[63] This concept was proposed based on the optimization of a structural model reported previously by using the generalized gradient approximation (GGA) in the Perdew–Burke–Ernzerhof (PBE) form. A dramatic structural change was observed. The new structure contains an Au core (with O_h point-group symmetry) of 14 atoms and six planar, ring-like gold-thiolate capping units, as shown in Fig. 1. In view of this structure, the Au atoms can be divided into two groups: 14 Au atoms formed the Au core in the Au(0) state (metallic state), and the remaining 24 Au formed an Au(I) thiolate species (in the oxidation state) capping the Au core. This new structure is closely related to the Garzón Au_{38} model,[62] which also incorporates the strong etching effects of thiol groups on the Au core in RS-AuNPs. Although the relative stability between the two models depends on the exchange correlation functional used, the finding of the formation of stable $[AuSR]_4$ units capped on a symmetric Au core not only supports the "divide-and-protect" concept, but also offers a new picture for understanding the bonding and structure of thiolate-protected gold nanoparticles. In 2007, a similar 'core-in-cage' model was also proposed to understand the structure of another magic-number RS-AuNP, $Au_{25}(SR)_{18}^-$,[85] which will be discussed in detail in the next section.

3.2 Two breakthroughs: the total structure determination of $Au_{102}(p\text{-MBA})_{44}$ and $Au_{25}(SCH_2CH_2Ph)_{18}^-$

Until 2007, $Au_{39}(PPh_3)_{14}Cl_6^{2+}$ held the record of the largest ligand-protected gold cluster that was successfully crystallized.[57] In October 2007, a research group led by Kornberg determined the atomic structure of an all-thiol-protected gold nanoparticle with 102 Au atoms, namely, $Au_{102}(p\text{-MBA})_{44}$, based on the single-crystal X-ray diffraction at 1.1 Å resolution.[64] Subsequently, a series of theoretical structural analyses of $Au_{102}(p\text{-MBA})_{44}$ were performed by Gao *et al.*, Han *et al.*, and Choi *et al.*, independently.[86–88] Choi *et al.* classified the Au atoms in $Au_{102}(p\text{-MBA})_{44}$ into three different shells through radial distance analysis: (1) the inner core consists of 39 Au atoms within 5.3 Å from the center of cluster; (2) the second shell consists of 40 Au atoms within a spherical shell of 6.1–6.4 Å from the center of cluster. The Au atoms in the second shell are connected to the S terminal of the –RS–Au–SR– staple motifs through a single Au–S bond. (3) The remaining 23 Au atoms occupy the outermost shell within a radius of 7.9–8.3 Å from the center, which form staple motif protection units.[87]

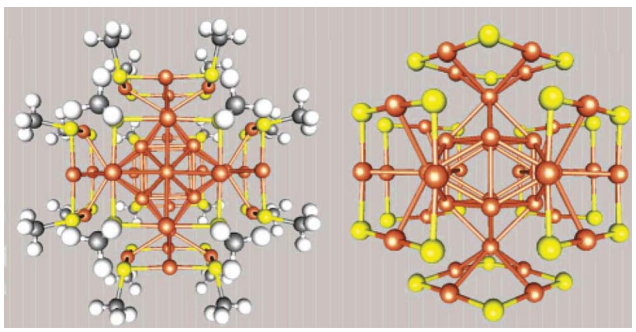

Fig. 1 Structural model for $Au_{38}(SMT)_{24}$ proposed by Häkkinen *et al.* Au, orange-brown; S, yellow; P, red; Cl, green; C, dark gray; H, white. The right hand model has the MT groups removed. Reprinted (adapted) with the permission of ref. 63. Copyright 2006 American Chemical Society.

Gao *et al.* provided an alternative view of the multi-layer structure of $Au_{102}(p\text{-MBA})_{44}$. From their structural analysis, the embedded Au_{102} cluster was decomposed into a multi-layered structure described as Au_{54}(penta-star)@Au_{38}(ten wings)@Au_{10}(two pentagon caps) as shown in Fig. 2.[86] The inner layer was an Au_{54} 'penta-star' consisting of five twinned Au_{20} tetrahedral subunits. Note that the tetrahedron Au_{20} is a magic-number structure of a free-standing gold cluster. Gao *et al.* pointed out that although a perfect T_d Au_{20} tetrahedral cluster is highly stable due to closure of the electronic shell, five perfect T_d Au_{20} clusters cannot completely form a perfect penta-star because of the deficiency in the solid-angle if the vertices of five T_d Au_{20} clusters are connected through the midpoint of the opposing edge. A stand-alone 54 Au-atom penta-star must be energetically unfavorable due to the large strain. Indeed, in the definition of the penta-star 54 atom Au core, the Au atom in part of the –RS–Au–SR– staple motif is taken into account. That is, each of the five vertices of the Au_{54} penta-star is a part of the –RS–Au–SR– staple motif covering the Marks decahedron Au core. Ultimately, the formation of a highly stable $Au_{102}(p\text{-MBA})_{44}$ nanocluster is a manifestation of a delicate (energetic) balance between local thiolate–gold interactions (in the form of staple motifs) with the growth mode compatible with the underlying Marks decahedral Au_{49} core.

The successful experimental determination and subsequent theoretical analysis of the atomic structure of $Au_{102}(p\text{-MBA})_{44}$ provides new knowledge about the structure of RS-AuNPs. The most important insight from these studies is that the interfacial structure in an RS-AuNP may be more complicated than previously expected: Au atoms on the surface of the Au core are lifted by thiol groups to form a certain number of protecting gold-thiolate staple-like motifs. If one studies the historic progress of the interfacial chemistry of thiol self-assembled monolayer (SAM) on Au surfaces, similar behavior of Au-SR interactions at the planar interface can be found.[84] As Au nanoparticles have larger curvatures than planar surfaces, much stronger interactions are expected at the interface between the thiol-ligands and Au core, consistent with previous theoretical models of $Au_{38}(SR)_{24}$. Another important finding is that the structure of $Au_{102}(p\text{-MBA})_{44}$ also supports the "divide-and-protect" concept.[63] However, the structure and number of staple motifs are still difficult to predict for an RS-AuNP like $Au_{38}(SR)_{24}$. The same problem exists for the determination of the geometry of the Au core in RS-AuNPs. Does an Au core always form a highly symmetric structure like the one in $Au_{102}(p\text{-MBA})_{44}$? Clearly, more atomic structures of RS-AuNPs are needed in order to derive more generic structural rules.

The determination of atomic structure of $Au_{25}(SR)_{18}^-$ is the second experimental breakthrough. For a long time, $Au_{25}(SR)_{18}^-$ had been incorrectly identified as $Au_{38}(SR)_{24}$.[21,37,89] In 2005, Tsukuda and co-workers corrected the mislabeled composition by

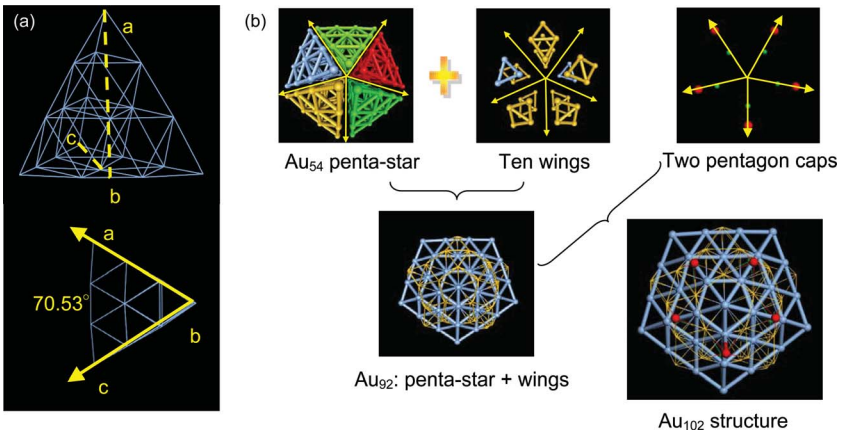

Fig. 2 Structural decomposition of an Au_{102} cluster. (a) Perfect tetrahedral T_d Au_{20}; (b) Graphitic anatomy of embedded Au_{102} structure. An Au_{54} penta-star consists of five twinned Au_{20} tetrahedral subunits. Reprinted (adapted) with permission from ref. 86. Copyright 2008 American Chemical Society.

electrospray ionization mass spectrometry (ESI-MS) measurement[90] of a series of electrophoretically fractionated NPs. The structural composition of the cluster is ascertained as $Au_{25}(SR)_{18}$. Extensive tests of the synthesis conditions and measurements affirm that the $Au_{25}(SG)_{18}$ (where SG denotes glutathione) is a stable magic-number cluster. In the meantime, theoretical efforts had also been made toward understanding the structure and magic-number nature of $Au_{25}(SG)_{18}$. In collaboration with Tsukuda, Nobusada *et al.* reported the first DFT calculation of the structure and electronic properties of $Au_{25}(SR)_{18}^{+}$ with R being simplified by a methyl group (MT).[85] In their theoretical study, the model still followed the conventional viewpoint of ligand protection on the metal clusters. Nobusada *et al.* constructed two types of Au_{25}-core, one with a face-centered-cubic (FCC) structure with six Au(111) facets consisting of eight gold atoms (FCC-Au_{25}-core), and another with a vertex-shared bi-icosahedral structure (SES-Au_{25}-core). The selection of SES-Au_{25}-core is partially motivated by the finding of a vertex-shared bi-icosahedral Au_{25}-core in $[Au_{25}(PPh_3)_{10}(SR)_5Cl_2]^{2+}$.[91] With both types of Au_{25}-core, the 18 thiol ligands were manually placed on the Au_{25}-core followed by a DFT optimization based on the Lee–Yang–Parr correlation functional (B3LYP). Surprisingly, the optimized structures from DFT showed the similar feature that part of the Au on the surface of the Au_{25}-core were etched by thiol groups to form gold-thiolate protecting units as that observed previously by Häkkinen *et al.* and Garzón *et al.* in their study of $Au_{38}(SR)_{24}$.[62,63] The most stable structure (FCC-2) with the lowest energy exhibited a clearly 'core-in-cage' structure, *i.e.*, an inner Au_7-core surrounded by $Au_{12}(SMT)_{12}$ and two $Au_3(SMT)_3$ rings.

Shortly after (in 2008), Akola *et al.* proposed an entirely new structural model[92] for $Au_{25}(SMT)_{18}^{-}$. The optimal structure model suggested by Akola *et al.* has an icosahedral Au_{13}-core that is protected by six –RS–Au–RS–Au–RS– staple motifs *via* the formation of 12 Au–S bonds at the core/ligand interface. The DFT calculation indicates the new model is much more stable than Nobusada's Au_{25} model, as shown in Fig. 3. The calculated binding energy of each –RS–Au–RS–Au–RS– complex to the Au_{13} core is 3.5 eV, much higher than that based on the FCC-2 model of Nobusada *et al.* (1.6 eV per $(AuSCH_3)_6$ oligomer). The simulated powder-XRD curve and UV-vis absorption spectra of various models also indicated that the combined icosahedrons Au_{13}-core and six –RS–Au–RS–Au–RS– staple motifs are in the best agreement with the experimental curves. Moreover, the absorption spectrum calculated from the TDDFT method suggested a HOMO–LUMO gap of 1.3 eV, in good agreement with the experimental measurement.

During the same time, the crystal structure of the $Au_{25}(SCH_2CH_2Ph)_{18}^{-}[Oct_4N]^{+}$ salt was successfully resolved independently by two experimental research groups.[66,67] Remarkably, the Au_{13}-core and semi-ring staple motif structures of $Au_{25}(SCH_2CH_2Ph)_{18}^{-}$ were in excellent agreement with the theoretical prediction. The discovery of the highly symmetric Au core with six extended –RS–Au–RS–Au–RS– motifs, as well as the finding of the atomic structure of $Au_{102}(p\text{-MBA})_{44}$, has stimulated considerable theoretical interest in exploring the structure and electronic properties of various RS-AuNPs.

3.3 Learning from nature: structural rules for thiolate-protected gold clusters

Based on the resolved atomic structures of $Au_{102}(p\text{-MBA})_{44}$ and $Au_{25}(SCH_2CH_2Ph)_{18}^{-}$, some generic structural features can be identified. First, both clusters exhibit a quasi-highly symmetric Au core, *i.e.* D_{5h} Au_{79}-core and I_h Au_{13}-core, respectively. Second, the Au cores are protected by a certain number of staple-like motifs through Au–S linkages, but the type and number of staple motifs are different. Due to the higher curvature of the

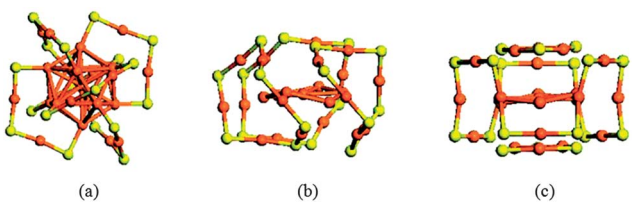

Fig. 3 (a) Akola's new structure model of $Au_{25}(SMT)_{18}^{-}$. (b) and (c) Nobusada's 'core-in-cage' models reported in 2007. The methyl groups are removed in all models. Reprinted (adapted) with permission from ref. 92. Copyright 2008 American Chemical Society.

icosahedral Au_{13}-core, the six protecting staple motifs are all in extended or dimeric form (–RS–Au–RS–Au–RS–) in $Au_{25}(SCH_2CH_2Ph)_{18}^-$, whereas the shorter monomeric –RS–Au–RS– staple motifs are dominant in $Au_{102}(p\text{-MBA})_{44}$ due to the relatively smaller curvature of the Au_{79}-core.

Jiang *et al.* performed a series of computational studies based on DFT/PBE calculations to understand how thiolate binds to gold atoms at a cluster surface.[93] In their first model, two isolated methyl thiol groups were closely placed on a truncated octahedral Au_{38} surface. After structural relaxation, a gold atom was lifted by two pre-adsorbed thiol groups and formed a monomeric –SR–Au–SR– motif. This investigation indicated that the formation of gold thiolate species is an energetically favorable process on the curved gold cluster. The energy analysis of a series of staple-covered $Au_{38}(MT)_x$ clusters for $x = 6$–24 indicated the adsorption energy per –SMT group decreases quickly with the increase of coverage of the –SMT group when x was less than 12. The maximum coverage for isolated staple motifs on an Au_{38} core is reached when x is about 20. With a further increase in the number of thiol ligands beyond 20, the dimerization of "staple" motifs (with a surface Au atom bonded to two terminals of –SR–Au–SR– motifs) was observed. Structural optimization of configurations of staple motifs and the Au core based on a simulated annealing approach yielded a more optimal structure whose electronic energy was 1.6 eV lower than the Häkkinen's model (2006).[63] In contrast to Häkkinen's model, the cyclic ring gold–thiolate motifs were no longer observed and the core structure was rather disordered. However, the agreement between the computed and measured optical absorption spectra was not so good. Shortly after, Jiang *et al.* proposed an improved structural model for $Au_{38}(MT)_{24}$, which was composed of a more symmetric Au_{12}-core and a series of monomeric and dimeric staple motifs. This new model yielded a further decrease in the total electronic energy, which was more stable than their earlier one by ~1.3 eV.[94]

Given the experimentally determined and theoretically predicted atomic structures of $Au_{25}(SCH_2CH_2Ph)_{18}^-$, $Au_{38}(SR)_{24}$, and $Au_{102}(p\text{-MBA})_{18}^-$, we have suggested a generic structural formula for RS-AuNPs similar to the "divide-and-protect" concept.[95] In view of the fact that both $Au_{25}(SCH_2CH_2Ph)_{18}^-$ and $Au_{102}(p\text{-MBA})_{18}$ can be decomposed into a highly symmetric Au_N core and a series of monomeric and dimeric protecting staple motifs, and that the staple motifs protect the symmetric Au_N-core through the formation of Au–S linkages on the outmost shell of the Au core, we introduce a general structure formula for RS-AuNP ($Au_m(SR)_n$) as $[Au]_{a+a'}[Au(SR)_2]_b[Au_2(SR)_3]_c$, where a, a', b and c are integers. The $[Au]_{a+a'}$ is the interior Au core and it satisfies a condition that the number of core 'surface' Au atoms (a') equals the sum of the end-points of the exterior motifs ($2b + 2c$), that is, each core surface Au atom is protected by one terminal of the staple motif. The values of a, a', b and c must satisfy $a + a' + b + 2c = m$ and $2b + 3c = n$ (constraint conditions). For example, the structure formula of $Au_{102}(SR)_{44}$ and $Au_{25}(SR)_{18}^-$ can be rewritten as $[Au]_{39+40}[Au(SR)_2]_{19}[Au_2(SR)_3]_2$ and $[Au]_{1+12}[Au_2(SR)_3]_6$, respectively. Note that for $Au_{102}(SR)_{44}$, one constraint condition, namely, $a' = 2b + 2c$, is not fully satisfied (as $a' = 40$, while $2b + 2c = 42$). This exception case is due to the fact that two Au atoms on the surface of the Au core are bonded with two S-terminals each. Tsukuda and co-workers proposed similar structural rules in their joint experimental and theoretical study of $Au_{38}(SR)_{24}$.[47] They proposed three simple structural principles: (1) a highly symmetric Au core; (2) the number of dimeric staple motifs increases with the decrease of cluster size; and (3) each surface Au atom is bound by one S-terminal of the staple motifs. Hereafter, we refer the structural formula and the three structural principles as the "inherent structure rule" for constructing a structural model of thiolate-protected gold clusters.

Based on the "inherent structure rule", five sets of structural divisions are suggested for $Au_{38}(SR)_{24}$: (i) $[Au]_{2+24}[Au(SR)_2]_{12}$, (ii) $[Au]_{3+22}[Au(SR)_2]_9[Au_2(SR)_3]_2$, (iii) $[Au]_{4+20}[Au(SR)_2]_6[Au_2(SR)_3]_4$, iv)$[Au]_{5+18}[Au(SR)_2]_3[Au_2(SR)_3]_6$ and (v) $[Au]_{6+16}[Au_2(SR)_3]_8$, all satisfying the constraint conditions.[95] Since the structures of the staple motif units are pre-defined, the structural prediction of $Au_{38}(SR)_{24}$ is simplified into a search for a reasonable structure for $[Au]_{2+24}$, $[Au]_{3+22}$, $[Au]_{4+20}$, and $[Au]_{5+18}$ that can match the geometry of the protecting staple motifs flawlessly. A set of initial $[Au]_{a+a'}$ ($a + a' = 22$–26) core structures are then built and they are covered by certain numbers of staple motifs, *e.g.* $[Au(SR)_2]$ and $[Au_2(SR)_3]$. The DFT optimizations are then applied to relax the proposed structures. We find that an isomeric structure whose group division is $[Au]_{5+18}[Au(SR)_2]_3[Au_2(SR)_3]_6$ exhibits exceptional stability, as shown in Fig. 4a. The Au_{23}-core can be viewed as a bi-icosahedral structure with two Au_{13} icosahedrons fused by an Au_3 face (Fig. 4b). The six $[Au_2(SR)_3]$ motifs are distributed evenly on two icosahedral Au_{13} subunits, with an additional three $[Au(SR)_2]$ motifs bridging the middle of Au core. The DFT calculation indicates that this new structure is 2.04 eV lower in energy than the lowest-energy structure previously reported. Electronic structure analysis further shows a HOMO–LUMO gap of about 0.9 eV. Further simulations of thw XRD curve and UV-vis absorption spectrum for the new structure indicates good agreements between experimental and theoretical results (Fig. 4c). The prediction of a face-fused bi-icosahedral Au core in $Au_{38}(SR)_{24}$ is interesting due to its close relation with the known icosahedral Au_{13}-core in $Au_{25}(SCH_2CH_2Ph)_{18}^-$ and reinforces the notion of a highly symmetric Au core for stabilizing the cluster structure. On the other hand, the ratio of monomeric and dimeric staple motifs (1.58) in the newly predicted structure is also within the two benchmark values corresponding to $Au_{25}(SCH_2CH_2Ph)_{18}^-$ (1.39) and $Au_{102}(p\text{-MBA})_{18}^-$ (2.32), a trend also noticed by Tsukuda *et al.*[47] All these analyses suggest this structural model should be very close to the realistic structure of $Au_{38}(SR)_{24}$.

In collaboration with Tsukuda and Häkkinen, Aikens *et al.* made a further improvement to the predicted structural model by making a number of different orientations of staple motifs.[96] It was found from previous experimental studies that the $Au_{38}(SG)_{24}$ exhibits strong circular dichroism (CD) signals which are five times stronger than those from $Au_{25}(SG)_{18}$.[14,19,97] The strong CD signals were assigned to metal-based transitions, which possibly included contributions from both the Au core and ligand-layer Au atoms. In our originally proposed Au_{38} model, the longer staple motif units are arranged in an idealized C_{3h} symmetry and the whole cluster exhibits a C_{3h} point-group symmetry. The TDDFT computation of the CD spectrum based on the C_{3h} model yields a rather weak rotatory strength (less than 50 esu^2 cm^2), which is inconsistent with the experimental observation. By changing the orientations of the staple motifs, Aikens and co-workers found a new D_3 symmetric structure with

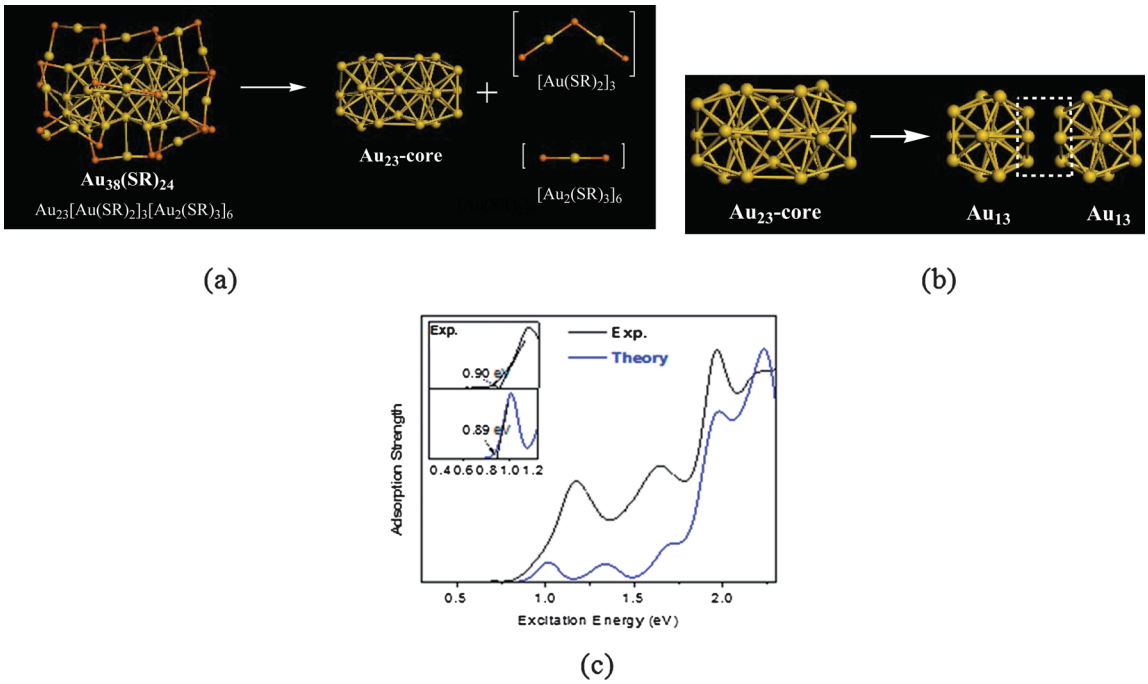

Fig. 4 (a) Face-fused structural model predicted for $Au_{38}(SR)_{24}$; (b) Structural pattern of bi-icosahedral Au_{23}-core. (c) Comparison of theoretical and experimental UV-vis absorption spectra. Reprinted (adapted) with the permission from ref. 95. Copyright 2008 American Chemical Society.

six –RS–Au–SR–Au–SR– motifs arranged in a zigzag form, which has an electronic energy ~0.3 eV lower than the previously reported model,[95] based on both LDA-Xα and PBE calculations with a triple-zeta polarized basis set. The computation of the CD spectrum of the improved model shows an increased rotatory strength below 2.2 eV.[96] The highest rotatory strength is seen at nearly 1.95 eV (~350 esu^2 cm^2), in agreement with the experimental observation.[14,97]

Jin and co-workers recently reported an improved synthesis method from which highly monodisperse, phenylethylthiolate-capped $Au_{38}(SC_2H_4Ph)_{24}$ clusters can be made (the yield increased to ~25%). This opened up a new possibility of crystallization of the clusters. Indeed, shortly after Aikens's publication, the crystallization of the atomically monodisperse $Au_{38}(SC_2H_4Ph)_{24}$ nanoparticles in a mixed solution of toluene and ethanol solution was achieved.[98] The X-ray crystallography revealed that the crystalline structure of $Au_{38}(SC_2H_4Ph)_{24}$ belongs to a triclinic space group P_1 and the unit cell contains a pair of enantiomeric clusters. Atomic structure analysis indicated that the $Au_{38}(SC_2H_4Ph)_{24}$ is composed of a face-fused bi-icosahedron Au_{23}-core and covered by six dimeric and three monomeric staple motifs, in good agreement with theoretical predictions.[95,96] However, the crystalline structure shows a slightly different arrangement of the dimeric staple motifs on the icosahedral Au_{13} unit from the theoretical models, that is, the six dimeric staples are arranged in a staggered fashion (Fig. 5) with an inversion center in the fused Au_3 plane.

3.4 Structural models for $Au_{12}(SC_2H_4Ph)_9^+$, $Au_{18}(SR)_{14}$, $Au_{20}(SC_2H_4Ph)_{16}$, $Au_{44}(SC_2H_4Ph)_{28}^{2-}$ and $Au_{144}(SR)_{60}$

The experimental confirmation of the theoretically predicted structure of $Au_{38}(SR)_{24}$ lends credence to the "inherent structure rule". Moreover, the confirmation of the bi-icosahedral Au_{23}-core in $Au_{38}(SR)_{24}$ validates the speculation of "atomic ordering" in Au cores of all highly stable thiolate-protected gold clusters.

Structural model for $Au_{144}(SR)_{60}$. Among the known series of highly stable thiolate-protected gold clusters, the 29 kDa gold nanoparticle has played an important role as it has been abundantly synthesized over a decade.[13] The structural composition of the 29 kDa nanoparticle was controversial and predicted to be in the range of 140–150 gold atoms and 50–60 thiolates.[47,99] Eventually, it was determined to be $Au_{144}(SR)_{60}$.[48] However, its atomic structure is still not fully resolved. Lopez-Acevedo *et al.* performed DFT calculations to investigate the structural and electronic properties of methylthiolate-protected Au_{144}.[100] The predicted structure of $Au_{144}(SMT)_{60}$ exhibits quasi I_h symmetry, as shown in Fig. 6a. A compact rhombicosi-dodecahedron 114-atom Au core was proposed in the structure. The 114-atom Au core is arranged into three concentric shells with 12, 42, and 60 Au atoms, respectively, and is protected by 30 equivalent monomeric staple motifs. The computed binding energy of each staple motif is 2.0 eV, much less than that of $Au_{25}(SMT)_{18}^-$ (3.5 eV).[92] The proposed structural model of the $Au_{144}(SMT)_{60}$ cluster is consistent with the "divide-and-protect" concept and the structural rule suggested. The cluster can be distinctly divided as $[Au]_{54+60}[Au(SR)_2]_{30}$, where the $[Au]_{54+60}$ core is highly symmetric (in the I_h point-group symmetry). The theoretically simulated XRD curve of the proposed cluster model shows good agreement with the experimental measurement (see Fig. 6b). In particular, a smaller shoulder peak between 5.5 and 6.0 nm^{-1} in the experimental curve is a hallmark of the icosahedron core, which is correctly reflected from the theoretical curve. The $Au_{144}(SR)_{60}$ has held the record for being the largest RS-AuNP whose structure has been predicted theoretically.

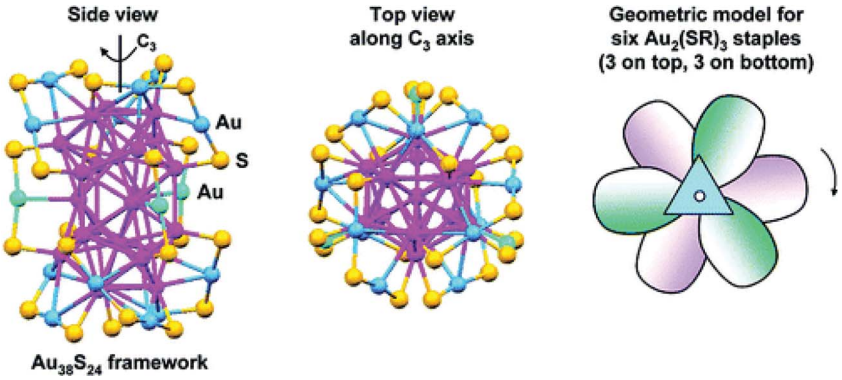

Fig. 5 Atomic structure of $Au_{38}(SC_2H_4Ph)_{24}$ resolved from the single-crystal XRD. Reprinted (adapted) with permission from ref. 98. Copyright 2010 American Chemical Society.

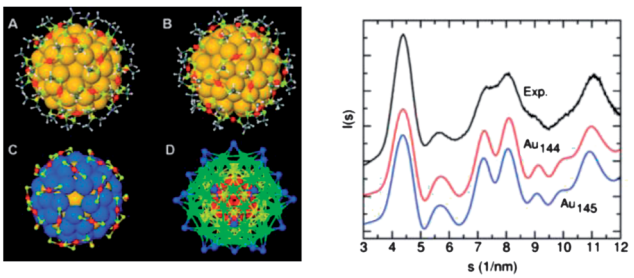

Fig. 6 (a) Relaxed structure of $Au_{144}(SR)_{60}$ viewed through a 5-fold (A) and a 3-fold (B) symmetry axis. Yellow: Au in the Au_{114} core; orange: Au in the RS–Au–SR unit; bright yellow: S; gray: C; white, H. (C) Arrangement of the RS–Au–SR units covering the 60-atom surface of the Au_{114} core (blue). (D) The 144 gold atoms shown in different shells. (b) Comparison of experimental and theoretical powder-XRD curves. Reprinted (adapted) with permission from ref. 100. Copyright 2009 American Chemical Society.

The smallest metal-rich thiolated gold nanocluster: $Au_{12}(SR)_9^+$. Jiang *et al.* attempted to theoretically resolve the smallest core-stacked RS-AuNP that was believed to have a highly symmetric Au core.[101] Note that the icosahedron and dodecahedron Au core structures have been shown in $Au_{25}(SR)_{18}^-$, $Au_{38}(SR)_{24}$ and $Au_{144}(SR)_{60}$, respectively, all belonging to the class of Platonic solids. However, the three remaining forms of Platonic solids: cube, tetrahedron and octahedron are yet to be observed or predicted in thiolate-protected gold clusters. As the cube is a rather open structure which is unlikely to be a good model for a compact Au core, the tetrahedron and octahedron Au cores were sought by Jiang *et al.*

Jiang *et al.* first investigated a tetrahedron-core-based $Au_8(SR)_6$ cluster that is composed of a tetrahedron Au_4 core and two dimeric staple motifs wrapping around two faces of the tetrahedron with the formation of four Au–S linkages.[101] However, their DFT optimizations resulted in a somewhat open structure with two dimeric staple motifs capping opposing edges of the tetrahedron Au core with a 90° Au–S–Au angle. Although their electronic structure calculations suggested a quite large HOMO–LUMO gap of 3.23 eV for the cluster, it was thought to be chemically unfavorable due to the open structure of the cluster (which may be prone to chemical attacks). The model was later revised by capping two opposite edges of the tetrahedron with the monomic staple motifs, *e.g.* $[Au(SR)_2]$. The optimized structure of neutral $[Au]_4[Au(SR)_2]_2$ or $Au_6(SR)_4$ has the tetrahedral Au_4-core with a slightly bent S–Au–S bond (~160°) in the staple motif. The cluster has a HOMO–LUMO gap of 2.40 eV and is thought to be a more realistic model compared to $Au_8(SR)_6$ due to the half-unprotected core. In their subsequent study of effects of the length of staple motifs on the stabilization of the smaller thiolate-protected gold clusters, Jiang *et al.* presented a new tetrahedron Au_4-core-based cluster, $Au_{10}(SR)_8$.[102] In this new cluster, the tetrahedron Au_4-core is wrapped by two extended trimeric staple motifs ($[Au_3(SR)_4]$). Geometric optimization and electronic calculation indicate that $Au_{10}(SR)_8$ is a good candidate that can accommodate a small tetrahedron Au_4-core.

To investigate the possible existence of an octahedron Au core in certain thiolate-protected gold clusters, Jiang *et al.* constructed an octahedron Au_6-core and used three dimeric staple motifs to cover the Au_6-core. The cluster is referred to as $Au_{12}(SR)_9$.[102] To remove the unpaired electron, a cation state of the cluster is investigated. After structural optimization, the optimized octahedral Au_8-core in $Au_{12}(SMT)_9^+$ is changed to D_{3d} point-group symmetry (within a 0.06 Å tolerance), and its six facets are effectively wrapped by the thiolate ligands as shown in Fig. 7a and b. Topologically, the $Au_{12}S_9$ framework in the optimized $Au_{12}(SMT)_9^+$ can be related to the familiar trefoil knot (Fig. 7c). Shortly after Jiang's theoretical prediction, an experimental isolation of $Au_{12}(SR)_9$ complexes (SR = *N*-acetylcysteine) was reported.[103]

Structural model for $Au_{44}(SR)_{28}^{2-}$. The all-aromatic monolayer-protected cluster (MPC) $Au_{44}(SPh)_{18}^{2-}$ was first isolated and characterized using mass spectroscopy with an 8.7 kDa mass in 2005 by Whetten and Price.[104] As the –PhS group possesses much higher electronegativity than alkanethiolates for its enhanced acidity (pKa = 6.6 *vs.* 9.4 for $-PhCH_2SH$), the question was raised as to whether the structure of the cluster could be understood based on the "inherent structure rule". Jiang *et al.* proposed a structural model for the $Au_{44}(SR)_{28}^{2-}$ by constructing two competing models:[105] one based on monomeric and dimeric motifs and another based on the longer oligomeric Au–SR motifs, first reported by Häkkinen.[63] Energy computations based on a DFT/PBE method indicate that the monomer–dimer

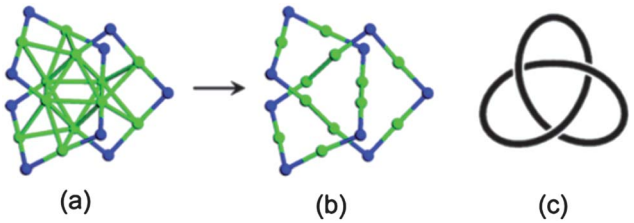

Fig. 7 (a) and (b) are the framework of $Au_{12}(SMT)_9^+$ proposed by Jiang *et al.* (c) A representation of cluster structure with a trefoil knot. Reprinted (adapted) with the permission from ref. 102. Copyright 2009 American Chemical Society. Au, green; S, blue.

model, consisting of an Au_{28}-core and 8 monomeric (–RS–Au–RS–) and 4 dimeric (–RS–Au–SR–Au–SR–) motifs (as shown in Fig. 8), is more stable by 2.0 eV than the polymer model that consists of an Au_{24}-core and a more diverse set of thiolate–gold oligomers. The monomer–dimer model is also found to give better agreement with experiment on the powder-XRD pattern. However, as pointed by the authors, the computed optical absorption spectra for both models are rather different from the experimental spectrum. Since the optical absorption spectra of RS-AuNPs are very sensitive to their structures, this result indicates that more appropriate models may exist. Recently, Dass *et al.* investigated the etching effects of the thiophenol ligand (–PhS) from a sample of a mixture that contains Au_{68} and Au_{102} as the precursor species.[106] In contrast to their early study of the etching effect of alkanethiolates (such as $-SCH_2Ph$) that leads to the formation of the stable $Au_{38}(SR)_{24}$ species,[107] the –PhS ligands demonstrate very different etching effects that eventually lead to the formation of a new stable RS-AuNP species, $Au_{36}(SPh)_{23}$.[106] The new experimental study reveals that the properties of the thiol ligand may strongly affect the stability and interfacial structure of RS-AuNPs. Can the proposed structural rule be applicable to such thiophenol ligand-protected gold nanoparticles? To answer this question, further experimental and theoretical studies on the structure of $Au_{36}(SPh)_{23}$ and $Au_{44}(SPh)_{28}^{2-}$ are needed.

Structural model of $Au_{20}(SR)_{16}$. The $Au_{20}(SCH_2CH_2Ph)_{16}$ cluster was first isolated by Jin and co-workers using a size-controlled synthesis approach.[49] The UV-vis absorption measurement indicates the cluster yields a step-wise, multiple-band optical absorption spectrum with a large HOMO–LUMO gap of 2.15 eV (the largest HOMO–LUMO gap that has ever been observed in synthetic thiolate-protected gold clusters). The $Au_{20}(SCH_2CH_2Ph)_{16}$ is extraordinarily robust against excess thiol etching, indicating its high stability, like $Au_{25}(SR)_{18}^-$.

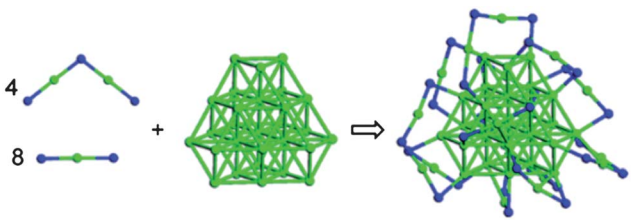

Fig. 8 Structural model of $Au_{44}(SMT)_{18}^{2-}$ constructed from the monomeric and dimeric staple motifs. Reprinted (adapted) with permission from ref. 105. Copyright 2010 American Chemical Society.

Moreover, the powder-XRD pattern also indicates the cluster may contain a loosely packed Au core due to the main peak at 3.85 nm^{-1}. However, the crystal structure of $Au_{20}(SCH_2CH_2Ph)_{16}$ has not been attained experimentally.

Theoretical efforts have been made to explain the packing style of the Au atoms in $Au_{20}(SCH_2CH_2Ph)_{16}$. In view of the relatively low Au : SR ratio in $Au_{20}(SR)_{16}$, both Pei *et al.* and Jiang *et al.* proposed the possible existence of much-extended staple motifs, *e.g.* –RS–Au–RS–Au–RS–Au–RS– or $[Au_3(SR)_4]$ in $Au_{20}(SCH_2CH_2Ph)_{16}$.[101,108] As such, the structural formula is expanded as $[Au]_{a+a'}[Au(SR)_2]_b[Au_2(SR)_3]_c$ $[Au_3(SR)_4]_d$, where the $[Au_2(SR)_3]$ type of staple motif was proposed for the first time. Considering the constraint conditions, only one division of $[Au]_{0+8}[Au_3(SR)_4]_4$ is allowed. Regarding the packing pattern of the Au core, Jiang *et al.* and Pei *et al.* suggested different models. Four structural forms of the Au_8 core, including the cube, T_d, cage, and fcc forms were proposed by Jiang *et al.* (see Fig. 9a).[101] Pei *et al.* suggested a much looser structure for the Au_8-core with a prolated shape, which can be viewed as the fusion of two tetrahedron Au_4 units through edges.[108] Three near-degenerate isomeric structures are attained (**Iso1–Iso3** as shown in Fig. 9b) based on the edge-fused Au_8-core. The electronic energy calculations (at the DFT/PBE level with the TZP basis set) with the –R group being simplified by a $-CH_3$ group indicate that Pei *et al.*'s model is slightly lower in energy by ~0.4 eV. Further calculations of the optical properties of the cluster indicate that the prolated Au_8-core-based model (**Iso2**) nearly reproduces the optical absorption gap and major peaks in the measured UV-vis absorption curve, as well as the overall patterns of the measured powder-XRD curve (Fig. 9c). The prolated Au_8-core-based model is considered as a leading candidate for the structure of $Au_{20}(SR)_{16}$.

Structural model for $Au_{18}(SR)_{14}$. In a recent paper on the synthesis of a mixture of thiolated gold clusters $Au_n(SR)_m$ (R = CH_2CH_2Ph) based on a surfactant-free synthesis method, Dass and co-workers reported that $Au_{18}(SCH_2CH_2Ph)_{14}$ exhibits peculiar stability and relatively high relative abundance in the matrix-assisted laser desorption time of flight mass spectrometry (MALDI-TOF-MS) in the size range of Au_{16}–Au_{31} cores.[109] The crystallization of this cluster, however, has not been achieved yet. According to the "inherent structure rule", the most likely structural formula for $Au_{18}(SR)_{14}$ is $[Au]_8[Au_3(SR)_4]_2[Au_2(SR)_3]_2$. Garzón *et al.* proposed a prolate-shaped bi-tetrahedron Au_8-core in $Au_{18}(SR)_{14}$,[110] similar to that in $Au_{20}(SR)_{16}$. The geometric optimization at the DFT/PBE level with the LANL2DZ (for Au) and 6-31g(d) (for other elements) basis sets suggests the lowest-energy isomer has a strongly distorted Au_8-core (in C_1 symmetry), covered by two dimeric and two trimeric staple motifs, as shown in Fig. 10. This structure is very different from that of the $Au_{20}(SR)_{16}$ cluster, whose inner Au_8-core exhibits near-D_{2d} symmetry. The strongly distorted Au core in $Au_{18}(SR)_{14}$ is attributed to the relatively short length of the two staple motifs. The predicted structure of $Au_{18}(SR)_{14}$ can be viewed as a reduced version of $Au_{20}(SR)_{16}$, where the two trimeric staple motifs in $Au_{20}(SR)_{16}$ are shortened to dimeric staple motifs. The reduced length of the staple motifs increases the stress in the cluster, resulting in a strongly distorted Au core in $Au_{18}(SR)_{14}$.

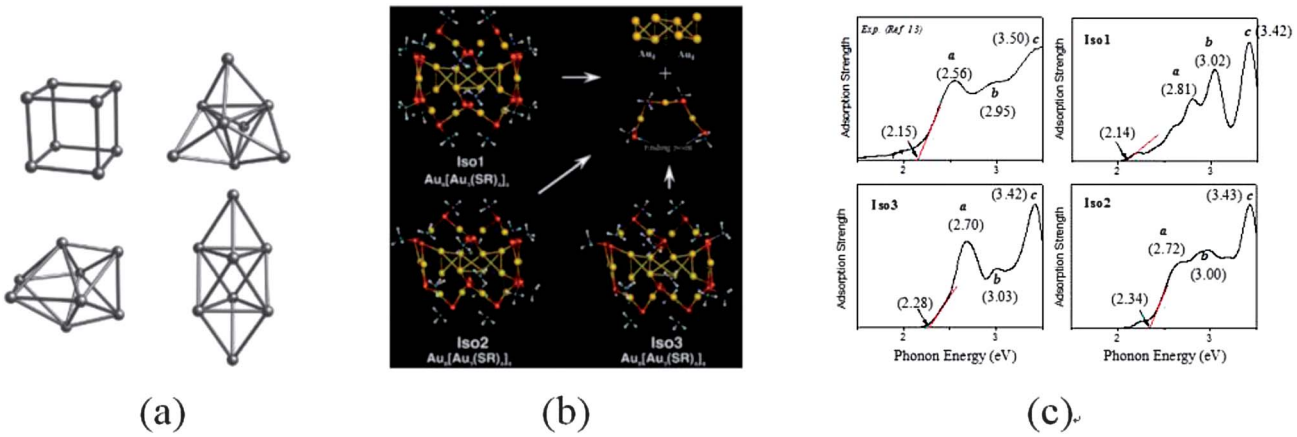

Fig. 9 (a) Au_8-core suggested by Jiang *et al.* [ref. 101]. (b) Low-energy isomer structures predicted by Pei *et al.* [ref. 108]. (c) Comparison of the theoretical UV–vis adsorption spectra of **Iso1–Iso3** with experiments. Reprinted (adapted) with permission from ref. 101 and 108. Copyright 2009 American Chemical Society.

The calculated UV-vis absorption spectra and powder-XRD curve based on the theoretical model for the $Au_{18}(SG)_{14}$ cluster indicate reasonable agreement with the experimental measurement. In particular, the calculated CD spectra have two positive and negative peaks in the 1.5–3.5 eV range, which are also in agreement with the experimental curve.[111] Nonetheless, by examining the energetics of the $Au_{18}(SR)_{14} + 2(AuSR)_4 \rightarrow Au_{20}(SR)_{16}$ reaction, where $(AuSR)_4$ is a cyclic tetramer and $Au_{20}(SR)_{16}$ is Pei *et al.*'s model,[108] Garzón *et al.* found an even higher stability by 0.45 eV for the $Au_{20}(SR)_{16}$ cluster in the presence of cyclic (AuSR).

3.5 'Staple fitness' and force-field based "divide-and-protect" scheme

The "inherent structure rule" and the "divide-and-protect" concept dramatically increase the likelihood of predicting the correct structural model for a thiolated gold nanoparticle. However, two more detailed questions arise when applying the rule and concept: (1) for a given symmetric Au core, several combinations of the arrangement of staple motifs are possible. How can one assign the most favorable arrangement? (2) There still exist many possibilities in constructing an Au_N-core that satisfies the proposed structural formula. How to construct more sensible Au core structures is another important question.

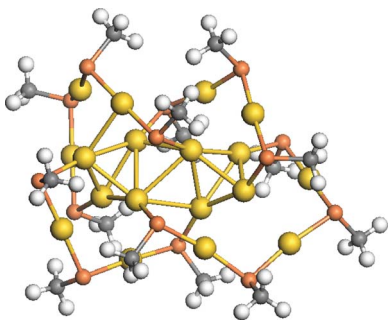

Fig. 10 (a) Structural model for $Au_{18}(SR)_{14}$ with –R is simplified by a methyl group. S atoms are in red, C atoms are in gray, and H atoms are in white. Au atoms in the dimer and trimer motifs are in orange and the core Au atoms are in yellow. Reprinted (adapted) with permission from ref. 110. Copyright 2012 Royal Society of Chemistry.

Jiang and Pei and their co-workers independently addressed the two questions in their recent theoretical studies of thiolate-protected gold clusters, concomitant with their structural predictions of two newly synthesized RS-AuNPs, $Au_{19}(SR)_{13}$ and $Au_{24}(SR)_{20}$, respectively. Jiang pointed out that a way to address the first question can be the concept of staple fitness.[112] For a given highly symmetric Au_N-core, the surface Au atoms on the core can be viewed as one-to-one dots that can bond to one S-atom terminal of the staple motifs. Since the staple motifs protect the Au core *via* S-atom terminals, a constraint must be enforced on the distance between the pair of surface Au atoms. For the monomeric and dimeric staple motifs, the head-to-tail distance usually falls into the range of 3.5 to 5.5 Å. Hence, two nearest-neighbor Au atoms with a distance of typically 2.8 Å cannot be connected by a staple motif. Therefore, one can set the nearest-neighbor distance in the Au core as a minimum distance constraint. By applying this constraint on distance, many combinations can be filtered out (a "pruning" process). The surviving combinations after the pruning process are ranked according to the total pair distance (TPD), which is defined as the sum of all inter-pair distances for a given combination of N pared-up dots. Taking the icosahedral Au_{13}-core as an example, on its surface the smallest nearest-neighbour Au–Au distance is 2.81 Å and the greatest Au–Au distance is 5.34 Å. There are 368 combinations of staple motifs within these two distance limits. The 368 combinations are then ranked by their TPD from high to low. The combinations of staple motifs having the greatest TPD are found to be in good agreement with the experimental structure. A similar approach can be applied to derive the arrangements of staple motifs on a bi-icosahedral Au_{23}-core for $Au_{38}(SR)_{24}$ from the nine theoretical models proposed previously by Pei *et al.* and by Aikens *et al.* The TPD measurement clearly indicates slight differences between the nine models.[95,96] The model with the greatest TPD value is indeed in good agreement with the experimental observation. These analyses suggest that the staple-fitness approach appears to be an efficient way to assign the most favorable mode of staple motif arrangement on a given Au core.

The staple-fitness method[112] has also been applied to predict the structure of a recently synthesized thiolate-protected gold cluster, $Au_{19}(SR)_{13}$. This cluster was isolated by Jin and co-workers using a kinetically controlled size-focusing synthesis and its structural composition was confirmed by mass spectroscopy characterizations.[113] By assigning the Au atoms into the core and staple motifs based on the proposed structural formula and constraints, two scenarios for the numbers of monomeric and dimeric motifs can be deduced: $[Au_{0+12}][Au(SR)_2]_5[Au_2(SR)_3]$ and $[Au_{1+10}]$ $[Au(SR)_2]_2[Au_2(SR)_3]_3$. By applying the staple-fitness method to a series of constructed highly symmetric Au cores, the lowest-energy structure derived from the fitness combination of staple motifs includes two monomeric staple motifs (which cap the two opposite concave regions of a vertex-truncated Au_{11}-core) and three dimer motifs (which protect the convex regions) (Fig. 11a and b). The simulated XRD curve (Fig. 11c) based on the optimized cluster is in good agreement with the experimental one, and the computed optical gap (1.3 eV) is also close to the experimental value (1.5 eV). In light of the predicted core structure of $Au_{19}(SR)_{13}$, the vertex-truncated icosahedral Au_{11}-core is closely related to that in $Au_{25}(SR)_{18}$. The $Au_{19}(SR)_{13}$ cluster is considered as an important intermediate towards the formation of $Au_{25}(SR)_{18}$ from smaller clusters.

To address the question of how to efficiently search for a reasonable structure of an Au core, we have recently proposed a classical force-field based "divide-and-protect" method.[114] The key steps involved in the force-field based "divide-and-protect" method are illustrated in Scheme 2. Any $Au_m(SR)_n$ cluster can be viewed as an Au_N-core fully protected by different staple motifs (*i.e.*, the "divide-and-protect" concept). Since the length and number of staple motifs are defined in the extended structural formula, *e.g.* $Au_{a+a'}[Au(SR)_2]_b[Au_2(SR)_3]_c[Au_3(SR)_4]_d\ldots$, where $Au_{a+a'}$ represents the Au core and *b*, *c* and *d* denote the number of different-sized staple motifs, the selection of different protecting staple motifs for a given cluster depends strongly on the ratio Au : SR. Typically, more extended staple motifs such as $[Au_3(SR)_4]$ and $[Au_4(SR)_5]$ *etc.* are only incorporated into the structural division when the ratio Au : SR is relatively small (*e.g.* <1.25). As structures of staple motifs are pre-defined, the structural prediction of RS-AuNPs turns into a search for the proper Au core structure ($Au_{a+a'}$) that matches the protecting staple motifs in a flawless fashion. The degrees of freedom for a cluster are thus reduced from $3m + 5n$ (with R = CH_3) to $3(a + a')$, for which the computational cost is dramatically reduced.

To seek the best Au core structure, the combined basin-hopping algorithm and empirical Sutton–Chen potential for Au–Au interactions are suggested. The empirical potential is much more efficient in generating highly symmetric Au core structures with less computational costs than *ab initio* methods. As reported previously, the classical potentials favor geometric packing of the gold atoms. The combination of the BH algorithm and the Sutton–Chen potential can quickly enumerate numerous desirable and highly symmetric Au core structures. From the generated structural database, one can therefore pick up some typical structures that satisfy the constraint conditions described in Section 3.3 for further assembly with the pre-defined staple motifs. The force-field based "divide-and-protect" approach has been validated with three benchmark models, $Au_{25}(SR)_{18}^-$, $Au_{38}(SR)_{24}$ and $Au_{102}(SR)_{44}$ whose Au core is I_h-Au_{13}, D_{3h}-Au_{23}, and D_{5h}-Au_{79}, respectively. The stable local minima, generated from the combined BH search and SC potential, are quite stable. Note that the DFT-based global search is less efficient for generating an Au core database due to the lack of symmetric Au cluster structures from the DFT-based search.

The force-field-based divide-and-protect approach has also been applied to determine the structure of another recently synthesized cluster, $Au_{24}(SR)_{20}$.[114] Because the ratio Au : S of $Au_{24}(SR)_{20}$ is slightly less than that of $Au_{20}(SR)_{16}$, which possesses a trimeric staple motif due to the relative small Au : S ratio (1.25), more extended staple motifs such as tetrameric and pentameric motifs ($[Au_4(SR)_5]$ and $[Au_5(SR)_6]$) should be incorporated into the structural divisions. By applying the "inherent structure rule", five structural divisions $Au_8[Au_3(SR)_4]_2[Au_5(SR)_6]_2$, $Au_8[Au_3(SR)_4][Au_4(SR)_5]_2[Au_5(SR)_6]$, $Au_8[Au_4(SR)_5]_4$, $Au_8[Au(SR)_2][Au_5(SR)_6]_3$ and $Au_8[Au_2(SR)_3][Au_4(SR)_5][Au_5(SR)_6]_2$ are considered, all containing an Au_8-core. Several Au_8-core structures are thus generated *via* the BH search with the SC potential. It is found that the D_{2d} symmetric Au_8-core protected by four pentameric staple motifs exhibits exceptional stability according to DFT calculations using different exchange-correlation functionals (PBE, TPSS,[115] and M06 (ref. 116)). This cluster also gives the best agreement between theoretical and experimental optical absorption spectra and XRD patterns among different isomer structures.

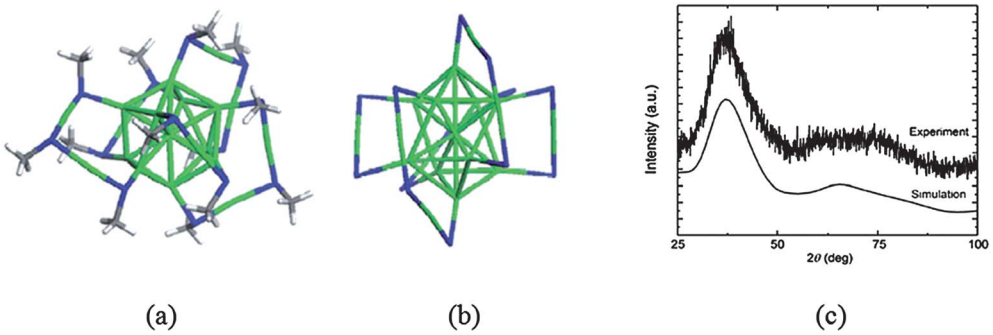

Fig. 11 Structural model for $Au_{19}(SR)_{13}$ (a) with or (b) without the representation of methyl groups. The S, C, H and Au atoms are in dark blue, gray, white and green, respectively. (c) Comparison of XRD curves from experimental measurement and theoretical simulation. Reprinted (adapted) with permission from ref. 112. Copyright 2011 John Wiley & Sons, Inc.

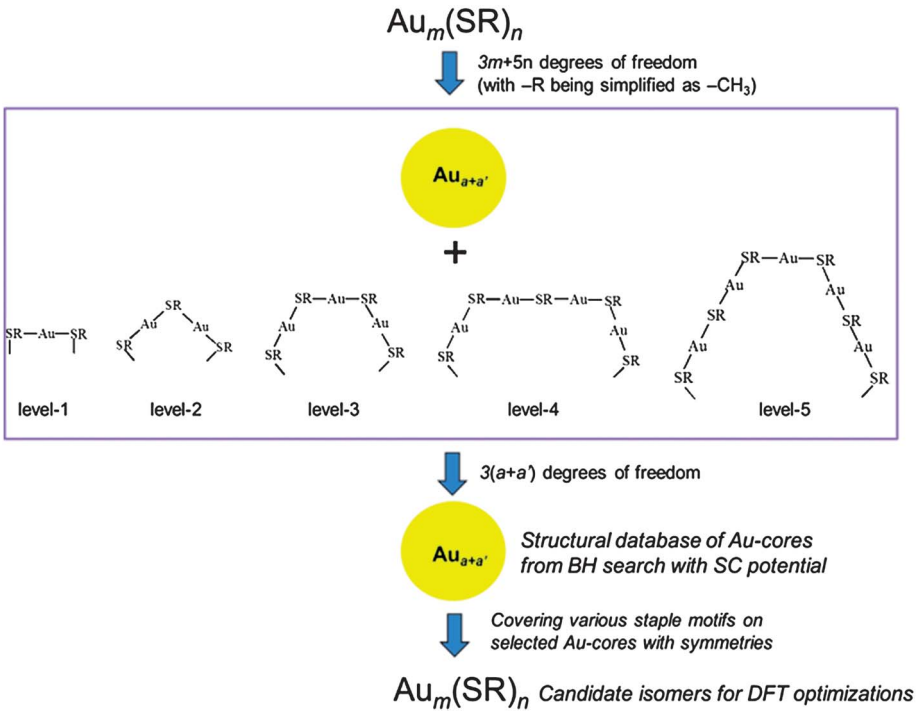

Scheme 2 Illustration of the force-field based divide-and-protect method. Reprinted (adapted) with permission from ref. 114 @ Copyright 2012 American Chemical Society.

Interestingly, the predicted lowest-energy structure of $Au_{24}(SR)_{20}$ has two tetrameric $[Au_3(SR)_4]$ and two pentameric $[Au_5(SR)_6]$ motifs interlocked like a linked chain from one end to another of the prolate Au_8-core, as shown in Fig. 12. One Au atom in the pentameric $[Au_5(SR)_6]$ motif is coordinated to four Au atoms in a tetrameric $[Au_3(SR)_4]$ motif, which is termed a catenane-like staple motif. Topologically, the predicted structure can be also viewed as a combination of two sets of symmetric interlocked oligomers $Au_5(SR)_4$ and $Au_7(SR)_6$. In fact, a recently proposed growth mechanism for RS-AuNPs indicates that $Au_n(SR)_{n-1}$ oligomers are likely to be formed during the initial growth of RS-AuNPs from the reduction of homoleptic Au(I) thiolates.[117]

In contrast to all previously determined or predicted structures of RS-AuNPs, the catenane-like staple motifs are only seen in the homoleptic Au(I) thiolates, which can exhibit either catenane, helix, or crown configurations.[118–120] The catenane-like staple motif in $Au_{24}(SR)_{20}$ is therefore considered as an intermediate structure that is part of the structural transition from a polymer chain-like form to a core-stacked form for thiolate-protected gold clusters. Here we define the core-stacked RS-AuNP by $Au_m(SR)_n$ with $m > n$. The finding of catenane-like staple motifs in $Au_{24}(SR)_{20}$ suggests that in the low Au : SR ratio limit (*i.e.*, approaching to 1 : 1), the interlocked staple motifs may become a prevalent conformation in RS-AuNPs. In fact, those isomers of $Au_{24}(SR)_{20}$ without the formation of catenane structures generally have higher energies, indicating the inter-locked structure is energetically favorable for thiolated gold clusters with a low Au : SR ratio.[114] Moreover, $Au_{24}(SR)_{20}$ has a similar bi-tetrahedron Au_8-core as that of $Au_{20}(SR)_{16}$. The tetrahedron Au_4-core has been predicted theoretically and observed experimentally for several small ligand-protected clusters such as $Au_{10}(SR)_8$ (ref. 101) (with Au : SR = 1.25) and $Au_4(PPh_3)_4^{2+}$.[121] On the other hand, a bi-pyramidal Au_6-core that has been previously predicted for $Au_{12}(SR)_9^+$ (with Au : SR = 1.33) and revealed in $Au_6(PPh_3)_6^{2+}$ can also be viewed as edge-fusion of two Au_4 units.[101,122] These analyses suggest that a major structural transition for the Au core may occur when the Au : SR ratio approaches the 1 : 1 limit. The close-packed tetrahedral Au_4 is thought of as a common unit for the Au core in small-sized RS-AuNPs with a relatively small Au : SR ratio (*e.g.*, <1.39).[114]

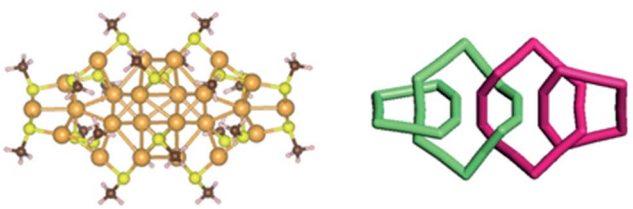

Fig. 12 Predicted structure model for $Au_{24}(SR)_{16}$ (left panel). The topological structural model with methyl groups are removed for clarity (right panel). The Au, S, C, and H atoms are in khaki, yellow, grey and white, respectively (left panel). Reprinted (adapted) with permission from ref. 114. Copyright 2012 American Chemical Society.

3.6 Structure of heteroatom-doped $Au_{25}(SR)_{18}^q$ ($q = -2, -1, 0, 1, 2$)

Heteroatom doping is an important way to modify the properties of metal clusters. For gas-phase gold clusters, a number of heterometal-doped Au clusters have been investigated *via* joint theoretical and experimental studies.[123,124] In the case of thiolate-protected gold clusters, Jiang *et al.* studied theoretically a set of

bi-metal $M@Au_{24}(SMT)_{18}^{q}$ clusters where M was the dopant metal atom that replaced the central Au atom in the 13-atom icosahedral core.[125,126] Different charge states ($q = -2, -1, 0, 1, 2$) were considered to preserve the 8e closed electron-shell according to the superatom model (see Section 4.1 below). It was found that metal atoms such as Pd, Pt, Ni, Cu, and Ag *etc.* led to stable cluster structures with the icosahedral core structure being well preserved. In particular, doping with a Pt atom (*i.e.* $Pt@Au_{24}(SMT)_{18}^{2-}$) yields a large HOMO–LUMO gap that is slightly larger than that of $Au_{25}(SCH_2CH_2Ph)_{18}^{-}$. Shortly after Jiang's theoretical prediction, several mass spectroscopy experiments showed that the $Au_{25}(SCH_2CH_2Ph)_{18}^{-}$ nanocluster can be doped by a single Pd (or Ag atom), becoming $Pd@Au_{24}(CH_2CH_2Ph)_{18}^{-}$.[127–131] Moreover, the one or two Pd-atom-doped $Pd_x@Au_{38-x}(SCH_2CH_2Ph)_{24}$ nanoclusters were also synthesized.[127,129] Kacprzak *et al.* and Walter *et al.* performed independent theoretical studies to determine the possible position of the doped metal atom in $M@Au_{24}(SMT)_{18}^{q}$. They found that the energetically most favorable position for the Pd atom was in the center of the icosahedral core, as supported by the good agreement between measured and computed optical absorption curves.[132,133] Other metal atoms such as Ag and Cr were suggested to replace Au atoms in the metal-thiolate ligand shell.

3.7 Structures of fragment clusters: $Au_mS_n^-$ and $Au_{21}(SR)_{14}^-$

Recent MALDI-MS experiments showed that fragments of $Au_{25}(SR)_{18}^-$ led to the formation of a series of high-abundance $Au_mS_n^-$ clusters.[134] Among them, the mono-anionic clusters $Au_{25}S_{12}^-$, $Au_{23}S_{11}^-$ and $Au_{27}S_{13}^-$ exhibit high stability. The formation of complex patterns of fragmented species includes many $Au_mS_n^+$ and $Au_mS_n^-$ clusters. A high abundance (magic number) of smaller $Au_mS_n^-$ clusters such as $Au_{13}S_8^-$, $Au_{12}S_8^-$ and $Au_6S_4^-$ was also observed in the fast-atom-bombardment MS of $Au_{25}(SR)_{18}^-$ in both positive and negative charge modes and in the ion-mobility MS of $Au_{25}(SR)_{18}^-$.[135–137]

Using the combined DFT and BH algorithm, a unique core-in-cage structure was found for $Au_{19}S_{12}^-$, $Au_{23}S_{11}^-$, $Au_{25}S_{12}^-$ and $Au_{27}S_{13}^-$ (Fig. 13a).[138] In such a core-in-cage structure, S atoms form the vertices of the cage and are connected by the Au atoms at the edges. The rest of the Au atoms form a symmetric core inside the cage. The core-in-cage structure of gold-sulfide clusters is distinct from the thiolate-protected gold clusters. A detailed study of the structural evolution of binary gold-sulfide cluster anions ($Au_mS_n^-$) in the smaller sizes was reported by us using a similar theoretical method.[139] Highly stable $Au_mS_n^-$ species such as $Au_6S_4^-$, $Au_9S_5^-$, $Au_9S_6^-$, $Au_{10}S_6^-$, $Au_{11}S_6^-$, $Au_{12}S_8^-$ and $Au_{13}S_8^-$ as detected in the ion mobility MS experiment of $Au_{25}(SCH_2CH_2Ph)_{18}$ were found to possess unique symmetric hollow cage structures such as quasi-tetrahedron, pyramidal, quasi-triangular prism, or quasi-cuboctahedron, respectively (Fig. 13b). The formation of these polyhedron structures were attributed to the high stability of the linear S–Au–S unit. An "edge-to-face" growth mechanism was also proposed to understand the structural evolution of small $Au_mS_n^-$ clusters from the quasi-tetrahedron to quasi-cuboctahedron structures.

The $Au_{21}(SCH_2CH_2Ph)_{14}^-$ was another magic-number cluster that was detected in MS experiments under several conditions.[127,135,136] From its structural composition, it can be viewed as the loss of an $[AuSR]_4$ fragment from the $Au_{25}(SR)_{18}^-$ cluster. The structure of $Au_{21}(SR)_{14}^-$ was examined recently based on DFT calculations from a step-by-step removal of an AuSR fragment from $Au_{25}(SR)_{18}^-$ according to the proposed structural principles.[140] A mechanism for the replacement of the dimeric motif $[Au_2(SR)_3]$ by the monomeric $[Au(SR)_2]$ motif was proposed as an energetically favorable process according to DFT calculations, which led to a structural model with an icosahedral Au_{13}-core covered by four monomeric and two dimeric staple motifs.

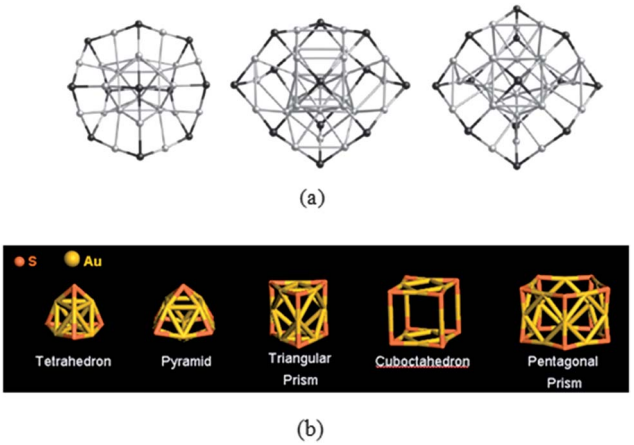

Fig. 13 (a) Core-in-cage models for $Au_{23}S_{11}^-$, $Au_{25}S_{12}^-$, and $Au_{27}S_{13}^-$. Adapted from ref. 138 @ Copyright 2011 John Wiley & Sons, Inc. (b) Hollow cage-like structures for $Au_6S_4^-$, $Au_9S_5^-$, $Au_9S_6^-$, $Au_{12}S_8^-$, and $Au_{15}S_{12}^-$. Reprinted (adapted) with permission from ref. 139. Copyright 2009 American Chemical Society.

4. Understanding the "magic" stability of thiolate-protected gold clusters

An interesting question related to the stability of thiolate-protected gold clusters is why the "staple motif" is common in these clusters. The formation of the staple motif units is largely caused by the strong Au–S interactions. With the decrease of the cluster's size, the increased curvature of the gold cluster renders the surface Au atom more reactive to the thiol groups. As demonstrated by Jiang's DFT calculations,[93] the formation of a staple motif protection unit is a spontaneous process when two thiol groups are closely adsorbed on a curved gold cluster surface. The high curvature of the nano-sized gold cluster is thus a key for the favorable formation of staple motif units. However, numerous experimental studies demonstrated a few clusters such as $Au_{25}(SR)_{18}$, $Au_{38}(SR)_{24}$ and $Au_{102}(SR)_{44}$ *etc.* exhibited extraordinary stabilities, or "magic" stability. To understand the intrinsic stability or "magic" stability of these clusters, both the electronic effects (the superatom model) and the thermodynamic factors have been taken into consideration.

4.1 Superatom model

The superatom model for metal clusters with a closed electron-shell structure was first proposed to explain the high abundance of certain magic-number alkali metal clusters ($N = 2$, 8, 18, 20, 40, and 58) observed in the MS experiments.[141] The model predicts that free valence electrons in a metal cluster may occupy

a set of orbitals that belong to an entire group of atoms rather than individual atoms separately (also known as a homogeneous electron gas or "jellium" model). The superatom model has been used to explain the electronic structures and high stabilities of certain ligand-protected gold clusters (such as $Au_{25}(SR)_{18}^{-}$, $Au_{102}(SR)_{44}$ and gold–phosphane–halide clusters) by Häkkinen *et al.* in 2008.[142]

The total number of free valence electrons (n^*) associated with a thiolate-protected gold cluster $Au_M(SR)_N^q$ can be counted based on the formula $n^* = M - N - q$, where M is the number of Au($6s^1$) electrons, N and q are the number of electron-withdrawing ligands (such as a thiol group) and the net charge of the cluster, respectively. From this electron counting formula, $Au_{25}(SR)_{18}^{-}$ and $Au_{102}(SR)_{44}$ have 8 and 58 free valence electrons, respectively, which are indeed the electronic magic numbers that correspond to a closed electron–shell within the framework of the spherical jellium model. Similarly, $Au_{12}(SR)_9^{+}$ and $Au_{44}(SR)_{28}^{2-}$ clusters also possess magic numbers of free valence electrons (2e and 18e, respectively) on the basis of the spherical jellium model. Earlier MS experiments by Whetten *et al.* revealed the existence of several magic-number clusters with 5, 8, 14, 22 and 28 kDa Au cores.[13,99] Among them, the 5, 8 and 28 kDa cores were assigned to Au_{25}, Au_{38}, and Au_{144}, respectively. Recently, a structural formula for the 14 kDa nanocluster was identified as $Au_{68}(SR)_{34}$ based on MALDI-TOF MS measurements.[143] The $Au_{68}(SR)_{34}$ cluster possesses a 38e electron shell according to the superatom model. Through an analysis of the angular momentum of Kohn–Sham orbitals, Häkkinen *et al.* presented evidence for the existence of a set of superatom orbtials in thiolate-protected gold clusters.[142] The reorganization of the electronic structures of the gold core upon passivation was shown in $Au_{102}(SR)_{44}$ from the 3S + 2D + 1H band of states.

Nonetheless, not all experimentally produced thiolate-protected gold clusters exhibit magic numbers of free valence electrons as described by the spherical jellium model. The $Au_{38}(SR)_{24}$ is a highly stable cluster that has been detected in many experiments under different reaction conditions, but the electron counting rule suggests it has fourteen free valence electrons that occupy the superatom orbitals. Similar situations were found for many other clusters such as $Au_{18}(SR)_{14}$ (4e), $Au_{19}(SR)_{13}$ (6e), $Au_{20}(SR)_{14}$ (4e), $Au_{24}(SR)_{16}$ (4e) and $Au_{144}(SR)_{60}$ (84e). The prediction of non-spherical Au cores in these clusters can be understood from a modified electron shell model. According to the ellipsoidal electron shell structure proposed by Clemenger,[144] a spherical superatom electron shell for a metal cluster can be further divided into several ellipsoidal subshells. An ellipsoidal electronic shell may explain the formation of a metal cluster with a non-spherical shape. The prolate shape of the Au cores in $Au_{20}(SR)_{14}$, $Au_{24}(SR)_{20}$ and $Au_{38}(SR)_{24}$ is consistent with this explanation.

Besides providing an explanation of the magic-numbers, electronic structures, and geometries of thiolate-protected gold clusters, the superatom model can be also used to understand the optical absorption, circular dichroism, and EPR spectra of the clusters. Based on both the superatom and ligand band orbitals, Aikens and co-workers reported a detailed theoretical analysis of the electronic excitation modes of several ligand-protected gold clusters such as $Au_{25}(SR)_{18}$ and $Au_{38}(SR)_{24}$.[68,96,145]

4.2 Thermodynamic and chemical analyses of RS-AuNPs

Although the superatom model can provide an explanation of the magic numbers and sizable HOMO–LUMO gaps of thiolated-gold clusters, it does not include the thermodynamic effect that may be another important factor that controls the stability of clusters. Thermodynamic and chemical analyses of the stability of the $Au_{102}(SR)_{44}$ cluster were performed by Reimers *et al.* and Han *et al.* based on DFT calculations.[146,147] By examining the thermodynamic stabilities of various structural models such as $Au_{79}(MT)_{40}$, $[Au_{79}(MT)_{40}]^{-}$, $Au_{102}(p\text{-MBA})_{44}$, $Au_{100}(MT)_{42}$, $Au_{102}(MT)_{44}$, and $Au_{104}(MT)_{46}$ through dissociation energy analysis, Reimers *et al.* found that the thermodynamic stability of these clusters varies considerably without an obvious correlation with the electronic shell closure.[146] The strong local chemical effects were suggested to regulate the chemical properties of the thiolate-protected gold clusters, in lieu of global electronic structures as described by the superatom model. Han *et al.* arrived at similar conclusions in their thermodynamic analysis of a series of thiolate-protected gold clusters with Au core sizes ranging from 98 to 106.[147] They suggested that the magic-number and high stability of the thiolate-protected gold cluster $Au_{102}(SMT)_{44}$ are not entirely due to the 58e closed electron shell or a relatively large HOMO–LUMO gap, because some other clusters with a similar Au core structure and a similar arrangement of staple motifs but without such a closed electron shell (*e.g.* $n^* \neq 58$) can possess an even larger HOMO–LUMO gap than $Au_{102}(SMT)_{44}$. Three factors were proposed to account for the high stability of $Au_{102}(SMT)_{44}$, namely, effective staple-motif formation, high stability against dissociation, and a large HOMO–LUMO gap.

5. Structure- and size-dependent catalytic activity of thiolate-protected gold clusters

It is well known that the bonding between metal and ligand generally involves electron transfer between the ligand and the metal. Such electron transfer enables the metal to carry a small amount of charge, which may significantly enhance the catalytic activity of metal clusters.[148] As an RS-AuNP consists of an inner Au core and outer staple motifs, the different charge state of the Au atoms in the ligand layer and in the gold core implies that they may undergo different degrees of chemical attack. To date, few theoretical and experimental studies of the catalytic mechanism of RS-AuNPs are reported. Several recent experimental studies show that $Au_{25}(SR)_{18}^{-}$ is an active catalyst in many organic reactions such as hydrogenation, styrene oxidation and O_2 activations.[149–152] The discovery of the conversion of anionic $Au_{25}(SCH_2CH_2Ph)_{18}^{-}$ to neutral $Au_{25}(SCH_2CH_2Ph)_{18}$ *via* air oxidation is very interesting because bare gold clusters in this size range are inert to O_2 activation.[151] Jin and co-workers proposed that the charged Au_{13}-core is a major active site for O_2 activation.[149,150] However, this mechanism has not been fully supported by theoretical calculations. Based on DFT calculations, Lopez-Acevedo *et al.* studied the catalytic activity of several ligand-protected gold clusters including $Au_{25}(SMT)_{18}^{-}$, $Au_{38}(SMT)_{24}$, $Au_{102}(SMT)_{44}$ and $Au_{144}(SMT)_{60}$.[152] Their DFT calculations indicate that the adsorption energy of an O_2 molecule on the Au_{13}-core is enhanced by the removal of one or two ligands from

the original thiolate-protected gold clusters, and is strongly dependent on the cluster size. The intact clusters without the removal of ligands indeed resist the O_2 adsorption. A nearly linear relationship between the HOMO–LUMO gap and the O_2 adsorption energy is derived. The electronic quantum-size effects (particularly the magnitude of the HOMO–LUMO gap) along with the defects on the clusters were concluded to be two critical factors for binding and reducing oxygen to a more active form. As many experimental observations show that the ligand shell is preserved during the catalytic reactions,[149–152] further theoretical studies on the catalytic mechanism of such ligand-protected gold clusters are needed to understand the role of cluster structure and ligands in various catalytic reactions.

6. Concluding remarks

The determination of the atomic structure of thiolate-protected gold clusters is of critical importance to the understanding of the physical and chemical properties of these special cluster species. Two recent breakthroughs in the determination of the atomic structures of $[Au_{25}(SCH_2CH_2Ph)_{18}]^q$ ($q = -1, 0$) and $Au_{102}(p\text{-MBA})_{44}$ from X-ray crystallography provide deeper insights into the structural properties of these complex clusters, as well as two benchmark systems for researchers to develop generic "inherent structure rules" for this class of clusters. The "inherent structure rule" has been found to be quite reliable in previous theoretical predictions of structural patterns in various synthesized thiolate-protected gold clusters. Theoretical studies have predicted a possible structural transition in thiolate-protected gold clusters with an Au : SR ratio close to 1 : 1, a phenomenon correlated with the initial nucleation stage in the growth of clusters. In particular, the prediction of much extended catenane-like staple motifs in $Au_{24}(SR)_{20}$ as well as common tetrahedral Au_4-units as the Au core in $Au_{12}(SR)_9^+$, $Au_{20}(SR)_{14}$ and $Au_{24}(SR)_{20}$ supports the existence of a major structural transition for thiolate-protected gold clusters at relatively small sizes. Moreover, the predicted truncated icosahedral Au_{12}-core and bi-icosahedral Au_{23}-core in $Au_{19}(SR)_{13}$ and $Au_{38}(SR)_{24}$, respectively, can be viewed as a manifestation of the structural evolution of Au cores from small-to-medium sizes. Despite notable progress in the predictive capability of atomic structures for thiolate-protected gold clusters, many research issues still need to be addressed. Among others, the most important need is continuous tests of the reliability of theoretical predictions. In Table 1, we provide a summary of the structural properties (determined from either experiments and/or theoretical predictions) of various alkylthiolate-protected gold clusters reported in the literature. To date, only two theoretical models, *i.e.* $Au_{25}(SR)_{18}^-$ and $Au_{38}(SR)_{24}$, have been successfully confirmed by experiments. Further experimental verification for the existence of extended "staple motifs" such as $[Au_3(SR)_4]$, and $[Au_5(SR)_6]$ are greatly needed to support theoretical predictions. Moreover, it remains unclear whether the theoretical basis of the "inherent structure rule" is universal for all types of thiol ligand-protected gold clusters such as $Au_{44}(SPh)_{24}^{2-}$ and $Au_{36}(SPh)_{23}$ with relatively stronger acidic –SPh groups. Another issue that remains to be addressed is the dynamic process of nucleation during the growth of thiolate-protected gold clusters from the reduced form of gold(I)–thiolate polymers. Aikens and co-workers have theoretically studied this process by examining the electron and hydride addition to gold(I)–thiolate oligomers ($Au_N(SR)_N$, $N = 3$–7).[153] The addition of a hydride ion to gold(I)–thiolate oligomers led to the production of free thiols and Au(0)-containing chain-like oligomers, which is considered as a possible intermediate for the

Table 1 A summary of the structural and electronic properties of various alkylthiolate-protected gold clusters reported in the literature. n^* represents the number of free valence electrons. The H–L gap refers to the energy gap between the highest occupied (HOMO) and lowest unoccupied molecular orbitals (LUMO). Clusters whose structures are predicted from theory or are still unknown are also listed

			Type and number of staple motifs						
RS-AuNPs	$N_{Au} : N_S$	Au core	–SR–Au–SR–	–SR–Au–SR–Au–SR–	–SR–Au–SR–Au–SR–Au–SR–	–SR–Au–SR–Au–SR–Au–SR–Au–SR–	–SR–Au–SR–Au–SR–Au–SR–Au–SR–Au–SR–	n^*	H–L Gap (eV)
$Au_{10}(SR)_{10}$ ref. 119	1.00	n/a	[0	0	0	0	0]	0	2.70
$Au_{24}(SR)_{20}$ ref. 114	1.20	Au_8	0	0	2	0	2	4	1.47
$Au_{20}(SR)_{16}$ ref. 108	1.25	Au_8	0	0	4	0	0	4	2.10
$Au_{18}(SR)_{14}$ ref. 110	1.29	Au_8	0	2	2	0	0	4	1.63
$Au_{12}(SR)_9^+$ ref. 102	1.33	Au_6	0	3	0	0	0	2	1.70
$Au_{25}(SR)_{18}^-$ ref. 66, 67 and 92	1.39	Au_{13}	[0	6	0	0	0]	8	1.33
$Au_{19}(SR)_{13}$ ref. 112	1.46	Au_{11}	2	3	0	0	0	6	1.50
$Au_{21}(SR)_{14}$ ref. 127, 135 and 136	1.50	Au_{13}	4	2	0	0	0	7	1.84
$Au_{44}(SR)_{28}^{2-}$ ref. 104 and 105	1.57	Au_{28}	8	4	0	0	0	18	1.60
$Au_{36}(SR)_{23}$ ref. 106	1.57	Unknown						13	0.90
$Au_{38}(SR)_{24}$ ref. 21, 22 and 25	1.58	Au_{23}	[3	6	0	0	0]	14	0.90
$Au_{40}(SR)_{24}$ ref. 154	1.67	Unknown						16	1.00
$Au_{68}(SR)_{34}$ ref. 143	2.00	Unknown						34	1.20
$Au_{102}(SR)_{44}$ ref. 64	2.32	Au_{79}	[19	2	0	0	0]	58	0.50
$Au_{144}(SR)_{60}$ ref. 48 and 100	2.40	Au_{114}	30	0	0	0	0	84	0
$Au_{333}(SR)_{79}$ ref. 155	4.22	Unknown						254	0

growth of nanoclusters. Nevertheless, how these Au(0)-containing intermediates further grow into a nanoparticle is still largely unknown. In particular, the origin of the preferential formation of the magic-number $Au_{25}(SR)_{18}^-$ cluster in most synthesis conditions deserves special attention from theorists. Finally, the catalytic mechanism and active sites on the clusters deserve focused study in the future. Recent experiments have revealed that thiolate-protected gold clusters are active in many organic catalytic reactions such as hydrogenation, styrene oxidation and O_2 activation.[149–151] Few theoretical studies have been reported on the origin of catalytic activity and the structure–activity relationship of these clusters. With more atomic structures of thiolate-protected gold clusters being determined, a better understanding of the structure–activity selectivity relationship is expected in the years to come.

Acknowledgements

YP is supported by the Natural Science Foundation of China (Grant No. 21103144) and Academic Leader Program in Xiangtan University (10QDZ34). XCZ is supported by grants from US NSF (EPS-1010094), ARL (W911NF1020099), and a seed grant by the Nebraska Center for Energy Sciences Research.

References

1 P. Gruene, D. M. Rayner, D. M. Redlich, A. F. G. van der Meer, J. T. Lynon, G. Meijer and A. Fielicke, *Science*, 2008, **321**, 674–676.
2 J. Li, X. Li, H.-J. Zhai and L.-S. Wang, *Science*, 2003, **299**, 864–867.
3 S. Bulusu, X. Li, L.-S. Wang and X. C. Zeng, *Proc. Natl. Acad. Sci. U. S. A.*, 2006, **103**, 8326–8330.
4 H. Häkkinen and U. Landman, *Phys. Rev. B: Condens. Matter*, 2000, **62**, R2287–2290.
5 F. Furche, R. Ahlrichs, P. Weis, C. Jacob, S. Glib, T. Bierweiler and M. M. Kappes, *J. Chem. Phys.*, 2002, **117**, 6982–6990.
6 W. Huang and L.-S. Wang, *Phys. Rev. Lett.*, 2009, **102**, 153401-1–153401-4.
7 M. Ji, X. Gu, X. Li, X. Gong, J. Li and L.-S. Wang, *Angew. Chem., Int. Ed.*, 2005, **44**, 7119–7123.
8 A. Lechtken, D. Schooss, J. R. Stairs, M. N. Blom, F. Furche, N. Morgner, O. Kostko, B. von Issendorff and M. M. Kappes, *Angew. Chem., Int. Ed.*, 2007, **46**, 2944–2948.
9 W. Huang, M. Ji, C.-D. Dong, X. Gu, L.-M. Wang, X. G. Gong and L.-S. Wang, *ACS Nano*, 2008, **2**, 897–904.
10 N. Shao, W. Huang, Y. Gao, L.-M. Wang, X. Li, L.-S. Wang and X. C. Zeng, *J. Am. Chem. Soc.*, 2010, **132**, 6596–6605.
11 P. Hohenberg and W. Kohn, *Phys. Rev.*, 1964, **136**, B864–871.
12 W. Kohn and L. J. Sham, *Phys. Rev.*, 1965, **140**, A1133–1138.
13 R. L. Whetten, J. T. Khoury, M. M. Alvarez, S. Murthy, I. Vezmar, Z. L. Wang, P. W. Stephens, C. L. Cleveland, W. D. Luedtke and U. Landman, *Adv. Mater.*, 1996, **8**, 428–433.
14 T. G. Schaaff, M. N. Shafigullin, J. T. Khoury, K. I. Vezmar, R. Whetten, W. G. Gullen and P. N. First, *J. Phys. Chem. B*, 1997, **101**, 7885–7891.
15 S. Chen, R. S. Ingram, M. J. Hostetler, J. J. Pietron, R. W. Murray, T. G. Schaaff, J. T. Khoury, M. M. Alvarez and R. L. Whetten, *Science*, 1998, **280**, 2098–2101.
16 A. C. Templeton, W. P. Wuelfing and R. W. Murray, *Acc. Chem. Res.*, 2000, **33**, 27–36.
17 R. Sardart, A. M. Funston, P. Mulvaney and R. W. Murray, *Langmuir*, 2009, **25**, 13840–13851.
18 M. Brust, M. Walker, D. Bethell, D. J. Schiffrin and R. Whyman, *J. Chem. Soc., Chem. Commun.*, 1994, 801–802.
19 R. Jin, H. Qian, Z. Wu, Y. Zhu, M. Zhu, A. Mohanty and N. Garg, *J. Phys. Chem. Lett.*, 2010, **1**, 2903–2910.
20 M. M. Alvarez, J. T. Khoury, T. G. Schaaff, M. N. Shafigullin, I. Vezmar and R. L. Whetten, *J. Phys. Chem. B*, 1997, **101**, 3706–3712.
21 T. G. Schaaff, G. Knight, M. N. Shafigullin, R. F. Borkman and R. L. Whetten, *J. Phys. Chem. B*, 1998, **102**, 10643–10646.
22 T. P. Bigioni, R. L. Whetten and O. Dag, *J. Phys. Chem. B*, 2000, **104**, 6983–6986.
23 R. H. Terrill, T. A. Postlethwaite, C. H. Chen, C. D. Poon, A. Terzis, A. D. Chen, J. E. Hutchison, M. R. Clark, G. Wignall, J. D. Londono, R. Superfine, M. Falvo, C. S. Johnson, E. T. Samulski and R. W. Murray, *J. Am. Chem. Soc.*, 1995, **117**, 12537–12548.
24 S. J. Green, J. J. Stokes, M. J. Hostetler, J. Pietron and R. W. Murray, *J. Phys. Chem. B*, 1997, **101**, 2663–2668.
25 R. S. Ingram, M. J. Hostetler, R. W. Murray, T. G. Schaaff, J. T. Khoury, R. L. Whetten, T. P. Bigioni, D. K. Guthrie and P. N. First, *J. Am. Chem. Soc.*, 1997, **119**, 9279–9280.
26 S. J. Green, J. J. Pietron, J. J. Stokes, M. J. Hostetler, H. Vu, W. P. Wuelfing and R. W. Murray, *Langmuir*, 1998, **14**, 5612–5619.
27 M. J. Hostetler, J. E. Wingate, C. J. Zhong, J. E. Harris, R. W. Vachet, M. R. Clark, J. D. Londono, S. J. Green, J. J. Stokes, G. D. Wignall, G. L. Glish, M. D. Porter, N. D. Evans and R. W. Murray, *Langmuir*, 1998, **14**, 17–30.
28 A. C. Templeton, M. J. Hostetler, C. T. Kraft and R. W. Murray, *J. Am. Chem. Soc.*, 1998, **120**, 1906–1911.
29 W. P. Wuelfing, S. M. Gross, D. T. Miles and R. W. Murray, *J. Am. Chem. Soc.*, 1998, **120**, 12696–12697.
30 S. W. Chen and R. W. Murray, *J. Phys. Chem. B*, 1999, **103**, 9996–10000.
31 J. F. Hicks, D. T. Miles and R. W. Murray, *J. Am. Chem. Soc.*, 2002, **124**, 13322–13328.
32 D. Lee, R. L. Donkers, G. L. Wang, A. S. Harper and R. W. Murray, *J. Am. Chem. Soc.*, 2004, **126**, 6193–6199.
33 R. Guo and R. W. Murray, *J. Am. Chem. Soc.*, 2005, **127**, 12140–12143.
34 G. L. Wang, T. Huang, R. W. Murray, L. Menard and R. G. Nuzzo, *J. Am. Chem. Soc.*, 2005, **127**, 812–813.
35 Y. Negishi and T. Tsukuda, *J. Am. Chem. Soc.*, 2003, **125**, 4046–4047.
36 H. Murayama, T. Narushima, Y. Negishi and T. Tsukuda, *J. Phys. Chem. B*, 2004, **108**, 3496–3503.
37 Y. Negishi, Y. Takasugi, S. Sato, H. Yao, K. Kimura and T. Tsukuda, *J. Am. Chem. Soc.*, 2004, **126**, 6518–6519.
38 Y. Negishi, K. Nobusada and T. Tsukuda, *J. Am. Chem. Soc.*, 2005, **127**, 5261–5270.
39 Y. Shichibu, Y. Negishi, T. Tsukuda and T. Teranishi, *J. Am. Chem. Soc.*, 2005, **127**, 13464–13465.
40 Y. Negishi, Y. Takasugi, S. Sato, H. Yao, K. Kimura and T. Tsukuda, *J. Phys. Chem. B*, 2006, **110**, 12218–12221.
41 Y. Negishi, H. Tsunoyama, M. Suzuki, N. Kawamura, M. M. Matsushita, K. Maruyama, T. Sugawara, T. Yokoyama and T. Tsukuda, *J. Am. Chem. Soc.*, 2006, **128**, 12034–12035.
42 H. Tsunoyama, Y. Negishi and T. Tsukuda, *J. Am. Chem. Soc.*, 2006, **128**, 6036–6037.
43 K. Ikeda, Y. Kobayashi, Y. Negishi, M. Seto, T. Iwasa, K. Nobusada, T. Tsukuda and N. Kojima, *J. Am. Chem. Soc.*, 2007, **129**, 7230–7231.
44 E. S. Shibu, M. A. H. Muhammed, T. Tsukuda and T. Pradeep, *J. Phys. Chem. C*, 2008, **112**, 12168–12176.
45 K. Nobusada, T. Tsukuda and N. Kojima, *J. Am. Chem. Soc.*, 2007, **129**, 7230–7231.
46 Y. Negishi, N. K. Chaki, Y. Shichibu, R. L. Whetten and T. Tsukuda, *J. Am. Chem. Soc.*, 2007, **129**, 11322–11323.
47 N. K. Chaki, Y. Negishi, H. Tsunoyama, Y. Shichibu and T. Tsukuda, *J. Am. Chem. Soc.*, 2008, **130**, 8608–8610.
48 H. Qian and R. Jin, *Nano Lett.*, 2009, **9**, 4083–4087.
49 M. Zhu, H. Qian and R. Jin, *J. Am. Chem. Soc.*, 2009, **131**, 7220–7221.
50 R. Jin, H. Qian, Z. Wu, Y. Zhu, M. Zhu, A. Mohanty and N. Garg, *J. Phys. Chem. Lett.*, 2010, **1**, 2903–2910.
51 H. Qian and R. Jin, *Chem. Mater.*, 2011, **23**, 2209–2217.
52 H. Qian, Y. Zhu and R. Jin, *J. Am. Chem. Soc.*, 2010, **132**, 4583–4585.
53 R. Jin, G. Wu, Z. Li, C. A. Mirkin and G. C. Schatz, *J. Am. Chem. Soc.*, 2003, **125**, 1643–1654.

54 M. Zhu, H. Qian, X. Meng, S. Jin, Z. Wu and R. Jin, *Nano Lett.*, 2011, **11**, 3963–3969.
55 G. Schmid, *Chem. Soc. Rev.*, 2008, **37**, 1909–1930.
56 C. E. Briant, R. C. Theobald, J. W. White, L. K. Bell and D. M. P. Mingos, *J. Chem. Soc., Chem. Commun.*, 1981, 201–206.
57 B. K. Teo, X. Shi and H. Zhang, *J. Am. Chem. Soc.*, 1992, **114**, 2743–2744.
58 M. C. Fairbanks, R. E. Benfield, R. J. Newport and G. Schmid, *Solid State Commun.*, 1990, **73**, 431–436.
59 D. Micheal and P. Mingos, *J. Chem. Soc., Dalton Trans.*, 1976, 1163–1169.
60 H. Häkkinen, R. N. Barnett and U. Landman, *Phys. Rev. Lett.*, 1999, **82**, 3264–3267.
61 A. Ulman, *Chem. Rev.*, 1996, **96**, 1533–1554.
62 L. Garzón, C. Rovira, K. Michaelian, M. R. Beltran, P. Ordejorn, J. Junquera, D. Sanchez-Portal, E. Artacho and J. M. Soler, *Phys. Rev. Lett.*, 2000, **85**, 5250–5251.
63 H. Häkkinen, M. Walter and H. Grönbeck, *J. Phys. Chem. B*, 2006, **110**, 9927–9931.
64 P. D. Jadzinsky, G. Calero, C. J. Ackerson, D. A. Bushnell and R. D. Kornberg, *Science*, 2007, **318**, 430–433.
65 R. L. Whetten and R. C. Price, *Science*, 2007, **318**, 407–408.
66 M. W. Heaven, A. Dass, P. S. White, K. M. Holt and R. W. Murray, *J. Am. Chem. Soc.*, 2008, **130**, 3754–3755.
67 M. Zhu, C. M. Aikens, F. J. Hollander, G. C. Schatz and R. Jin, *J. Am. Chem. Soc.*, 2008, **130**, 5883–5885.
68 C. M. Aikens, *J. Phys. Chem. Lett.*, 2011, **2**, 99–104.
69 H. Häkkinen, *Chem. Soc. Rev.*, 2008, **37**, 1847–1859.
70 D. Jiang, *Acta Phys.-Chim. Sin.*, 2010, **26**, 999–1016.
71 A. P. Sutton, *Philos. Mag. Lett.*, 1990, **61**, 139–164.
72 R. P. Gupta, *Phys. Rev. B*, 1981, **23**, 6265–6270.
73 N. T. Wilson and R. L. Johnston, *Eur. Phys. J. D*, 2000, **12**, 161–169.
74 L. Garzön, K. Michaelian, M. R. Beltrán, A. Posada-Amarillas, P. Ordejón, E. Artacho, D. Sanchez-Portal and J. M. Soler, *Eur. Phys. J. D*, 1999, **9**, 211–215.
75 M. Born and J. R. Oppenheimer, *Ann. Phys.*, 1927, **389**, 457–484.
76 B. Hartke, *J. Phys. Chem.*, 1993, **97**, 9973–9976.
77 S. Kirkpatrick, C. D. Gelatt and M. P. Vecchi, *Science*, 1983, **220**, 671–680.
78 D. J. Wales and J. P. K. Doye, *J. Phys. Chem. A*, 1997, **101**, 5111–5116.
79 E. Runge and E. K. U. Gross, *Phys. Rev. Lett.*, 1984, **52**, 997–1000.
80 W. D. Luedtke and U. Landman, *J. Phys. Chem. A*, 1996, **100**, 13323–13329.
81 N. T. Wilson and R. L. Johnston, *Phys. Chem. Chem. Phys.*, 2002, **4**, 4168–4171.
82 C. Majumder, T. M. Briere, H. Mizuseki and Y. Kawazoe, *J. Chem. Phys.*, 2002, **117**, 2819–2822.
83 A. Larsson, M. Nolan and J. C. Greer, *J. Phys. Chem. B*, 2002, **106**, 5931–5937.
84 P. Maksymovych, D. C. Sorescu and J. T. Yates, *Phys. Rev. Lett.*, 2006, **97**, 146103–146106.
85 T. Iwasa and K. Nobusada, *J. Phys. Chem. C*, 2007, **111**, 45–49.
86 Y. Gao, N. Shao, X. C. Zeng and X. C., *ACS Nano*, 2008, **2**, 1497–1503.
87 Y.-K. Han, H. Kim, J. Jung and Y. C. Choi, *J. Phys. Chem. C*, 2010, **114**, 7548–7552.
88 T. Li, G. Galli and F. Gygi, *ACS Nano*, 2008, **2**, 1896–1902.
89 R. L. Donkers and R. W. Murray, *Langmuir*, 2004, **20**, 1945–1952.
90 Y. Negishi, K. Nobusada and T. Tsukuda, *J. Am. Chem. Soc.*, 2005, **127**, 5261–5270.
91 Y. Schichibu, Y. Negishi, T. Watanabe, N. K. Chaki, H. Kawaguchi and T. Tsukuda, *J. Phys. Chem. C*, 2007, **111**, 7845–7847.
92 J. Akola, M. Walter, R. L. Whetten, H. Hakkinen and H. Grönbeck, *J. Am. Chem. Soc.*, 2008, **130**, 3756–3757.
93 D. Jiang, M. L. Tiago, W. D. Luo and S. Dai, *J. Am. Chem. Soc.*, 2008, **130**, 2777–2779.
94 D. Jiang, W. Luo, M. L. Tiago and S. Dai, *J. Phys. Chem. C*, 2008, **112**, 13905–13910.
95 Y. Pei, Y. Gao and X. C. Zeng, *J. Am. Chem. Soc.*, 2008, **130**, 7830–7832.
96 O. Lopez-Acevedo, H. Tsunoyama, T. Tsukuda, H. Häkkinen and C. M. Aikens, *J. Am. Chem. Soc.*, 2010, **132**, 8210–8218.
97 T. G. Schaaff and R. L. Whetten, *J. Phys. Chem. B*, 2000, **104**, 2630–2641.
98 H. Qian, W. T. Eckenhoff, Y. Zhu, T. Pintauer and R. Jin, *J. Am. Chem. Soc.*, 2010, **132**, 8280–8281.
99 T. G. Schaaff, M. N. Shafigullin, J. T. Khoury, I. Vezmar and R. L. Whetten, *J. Phys. Chem. B*, 2001, **105**, 8785–8796.
100 O. Lopez-Acevedo, J. Akola, R. L. Whetten, H. Grönbeck and H. Häkkinen, *J. Phys. Chem. C*, 2009, **113**, 5035–5038.
101 D. Jiang, W. Chen, R. L. Whetten and Z. Chen, *J. Phys. Chem. C*, 2009, **113**, 16983–16987.
102 D. Jiang, R. L. Whetten, W. Luo and S. Dai, *J. Phys. Chem. C*, 2009, **113**, 17291–17295.
103 Y. Zhang, S. Shuang, C. Dong, C. K. Lo, M. C. Paau and M. M. F. Choi, *Anal. Chem.*, 2009, **81**, 1676–1685.
104 R. C. Price and R. L. Whetten, *J. Am. Chem. Soc.*, 2005, **127**, 13750–13751.
105 D. Jiang, M. Walter and J. Akola, *J. Phys. Chem. C*, 2010, **114**, 15883–15889.
106 P. R. Nimmala and A. Dass, *J. Am. Chem. Soc.*, 2011, **133**, 9175–9177.
107 A. C. Dharmaratne, T. Krick and A. Dass, *J. Am. Chem. Soc.*, 2009, **131**, 13604–13605.
108 Y. Pei, Y. Gao and X. C. Zeng, *J. Am. Chem. Soc.*, 2009, **131**, 13619–13621.
109 S. M. Reilly, T. Krick and A. Dass, *J. Phys. Chem. C*, 2010, **114**, 741–745.
110 A. Tlahuice and I. L. Garzon, *Phys. Chem. Chem. Phys.*, 2012, **14**, 3737–3740.
111 T. Tsukuda, H. Tsunoyama and Y. Negishi, in *Metal Nanoclusters in Catalysis and Materials Science: The Issue of Size Control*, ed. B. Corain, G. Schmid and M. Toshima, Elsevier, Amsterdam, 2008, p. 373.
112 D. Jiang, M. Walter and J. Akola, *Chem.–Eur. J.*, 2011, **17**, 12289–12293.
113 Z. Wu, M. A. MacDonald, J. Chen, P. Zhang and R. Jin, *J. Am. Chem. Soc.*, 2011, **133**, 9670–9673.
114 Y. Pei, R. Pal, C. Liu, Y. Gao, Z. Zhang and X. C. Zeng, *J. Am. Chem. Soc.*, 2012, **134**, 3015–3024.
115 V. N. Staroverov, G. E. Scuseria, J. Tao and J. P. Perdew, *J. Chem. Phys.*, 2003, **119**, 12129–12137.
116 Y. Zhao and D. G. Truhlar, *J. Chem. Phys.*, 2006, **125**, 194101–194118.
117 B. M. Barngrover and C. M. Aikens, *J. Phys. Chem. Lett.*, 2011, **2**, 990–994.
118 R. Wiseman, P. A. Marsh, P. T. Bishop, B. J. Brisdon and M. F. Mahon, *J. Am. Chem. Soc.*, 2000, **122**, 12598–12599.
119 N. Shao, Y. Pei, Y. Gao and X. C. Zeng, *J. Phys. Chem. A*, 2009, **113**, 629–632.
120 H. Grönbeck, M. Walter and H. Häkkinen, *J. Am. Chem. Soc.*, 2006, **128**, 10268–10275.
121 E. Zeller, H. Beruda and H. Schmidbaur, *Inorg. Chem.*, 1993, **32**, 3203–3204.
122 C. E. Briant, K. P. Hall, D. M. P. Mingos and A. C. Wheeler, *J. Chem. Soc., Dalton Trans.*, 1986, 687–692.
123 Y. Gao, S. Bulusu and X. C. Zeng, *J. Am. Chem. Soc.*, 2005, **127**, 15680–15681.
124 L.-M. Wang, S. Bulusu, H.-J. Zhai, X. C. Zeng and L. S. Wang, *Angew. Chem., Int. Ed.*, 2007, **46**, 2915–2918.
125 D. Jiang and S. Dai, *Inorg. Chem.*, 2009, **48**, 2720–2722.
126 D. Jiang and R. L. Whetten, *Phys. Rev. B: Condens. Matter Mater. Phys.*, 2009, **80**, 115402–115406.
127 H. Qian, E. Barry, Y. Zhu and R. Jin, *Acta Phys.-Chim. Sin.*, 2011, **27**, 513–519.
128 Y. Negishi, K. Igarashi, K. Munakata, W. Ohgake and K. Nobusada, *Chem. Commun.*, 2012, **48**, 660–662.
129 Y. Negishi, T. Iwai and M. Ide, *Chem. Commun.*, 2010, **46**, 4713–4715.
130 Y. Negishi, W. Kurashige, Y. Niihori, T. Iwasa and K. Nobusada, *Phys. Chem. Chem. Phys.*, 2010, **12**, 6219–6225.
131 F. Parker, J. E. F. Weaver, F. McCallum, C. A. Fields-Zinna and R. W. Murray, *Langmuir*, 2010, **26**, 13650–13654.
132 A. Kacprzak, L. Lehtovaara, J. Akola, O. Lopez-Acevedoa and H. Häkkinen, *Phys. Chem. Chem. Phys.*, 2009, **11**, 7123–7129.
133 M. Walter and M. Moseler, *J. Phys. Chem. C*, 2009, **113**, 15834–15837.
134 Z. Wu and R. Jin, *ACS Nano*, 2009, **3**, 2036–2042.

135 A. Dass, G. B. Dubay, C. A. Fields-Zinna and R. W. Murray, *Anal. Chem.*, 2008, **80**, 6845–6851.
136 A. Angel, L. T. Majors, A. C. Dharmaratne and A. Dass, *ACS Nano*, 2010, **4**, 4691–4700.
137 Z. H. Tang, B. Xu, B. H. Wu, D. Robinson, N. Bokossa and G. L. Wang, *Langmuir*, 2011, **27**, 2989–2996.
138 D. Jiang, S. Walter and S. Dai, *Chem.–Eur. J.*, 2010, **16**, 4999–5003.
139 Y. Pei, N. Shao, H. Li, D. Jiang and X. C. Zeng, *ACS Nano*, 2011, **5**, 1441–1449.
140 O. Lopez-Acevedo and H. Häkkinen, *Eur. Phys. J. D*, 2011, **63**, 311–314.
141 R. I. G. Hughes, *Perspect. Sci.*, 2006, **14**, 457–524.
142 M. Walter, J. Akola, O. Lopez-Acevedo, P. D. Jadzinsky, G. Calero, C. J. Ackerson, R. L. Whetten, H. Gronbeck and H. Hakkinen, *Proc. Natl. Acad. Sci. U. S. A.*, 2008, **105**, 9157–9162.
143 A. Dass, *J. Am. Chem. Soc.*, 2009, **131**, 11666–11667.
144 K. Clemenger, *Phys. Rev. B*, 1985, **32**, 1359–1362.
145 C. M. Aikens, *J. Phys. Chem. C*, 2008, **112**, 19797–19800.
146 J. R. Reimers, Y. Wang, B. O. Cankurtaran and M. J. Ford, *J. Am. Chem. Soc.*, 2010, **132**, 8378–8384.
147 Y.-K. Han, H. Kim, J. Jung and Y. C. Choi, *J. Phys. Chem. C*, 2010, **114**, 7548–7552.
148 B. Yoon, H. Häkkinen, U. Landman, A. S. Wörz, J.-M. Antonietti, S. Abbet, K. Judai and U. Heiz, *Science*, 2005, **307**, 403–407.
149 Y. Zhu, H. Qian and R. Jin, *Chem.–Eur. J.*, 2010, **16**, 11455–11462.
150 Y. Zhu, H. Qian, M. Zhu and R. Jin, *Adv. Mater.*, 2010, **22**, 1915–1920.
151 M. Zhu, W. T. Eckenhoff, T. Pintauer and R. Jin, *J. Phys. Chem. C*, 2008, **112**, 14221–14224.
152 O. Lopez-Acevedo, K. A. Kacprzak, J. Akola and H. Häkkinen, *Nat. Chem.*, 2010, **2**, 329.
153 A. M. Barngrover and C. M. Aikens, *J. Phys. Chem. Lett.*, 2011, **2**, 990–994.
154 H. Qian, Y. Zhu and R. Jin, *J. Am. Chem. Soc.*, 2010, **132**, 4583–4585.
155 H. Qian, Y. Zhu and R. Jin, *Proc. Natl. Acad. Sci. U. S. A.*, 2012, **109**, 696–700.

